

1.1 Introduction:

Frustrated spin systems have recently attracted considerable attention because of their fascinating magnetic and multiferroic properties. The Delafossites (ABO_2 -type materials, $A=Cu, Ag, Pd..$; B-transition metals) where A cations are linearly coordinated with two oxygen ions while B cations are situated in distorted edge-sharing BO_6 octahedra. $CuFeO_2, CuCrO_2$ having delafossites structure while $CuMnO_2$ exhibit distorted delafossite or Crednerite structure which belongs to frustrated spin system. $CuFeO_2$ and $CuCrO_2$ are triangular lattice antiferromagnet, in which antiferromagnetic interactions between the magnetic Fe^{3+} or Cr^{3+} ions forming the perfect triangular lattice. Credenerite structure $CuMnO_2$ comprising isosceles-triangular lattice which occurs due to Jahn-Teller distortion of $Mn^{3+}(3d^4:t_{2g}^3e_g^1)$ with an orbital degree of freedom. Since these systems have strong magnetic frustration therefore they exhibit a variety of unconventional magnetic phase transitions. Geometrical frustration is an important characteristic in magnetism which rely on relative orientations of spins. In such systems, frustration is caused by either competing interactions or lattice geometries, which is not allowed to the energy minimization of all spin pairs simultaneously, resulting a large number of degenerate spin configurations. Consequently, these system possess unconventional magnetic states, such as Spin glass, Griffith phase, Exchange bias, Spin liquid etc. As in the case of two dimensional triangular lattice in which three magnetic ions situated on the corners of a triangle having antiferromagnetic interaction between them, the energy is minimized or ground state (because every physical phenomena is towards achieving the stability and the minimizing the energy) when each spin is aligned opposite to neighbours once the first two spins align antiparallel, the third one is being frustrated as its two possible orientations up and down give the same energy. In a three-dimensional system of corner sharing tetrahedra, at least two antiferromagnetic bonds are always frustrated. The only constraint on the ground state of such systems is the vector sum of the spins on a frustrated unit (triangle or tetrahedron) is zero. Also in case of tetrahedron in 3D in which four spins arranged in a corner of tetrahedron may experience geometric frustration. There are six nearest neighbour interactions, four of which are antiparallel and thus favourable but two of which

(between 1&2 and 3&4) are unfavorable as is shown in fig.1.1(c). So it is impossible to have all interactions favourable and the system becomes frustrated. In case of square lattice, each nearest neighbour interaction is antiferromagnetic leads to being unfrustrated. In two dimension, a section of Kagome lattices in which corner sharing triangular lattice system may experience geometric frustration. The pyrochlore lattice having $A_2B_2O_7$ formula unit, fig.1.1(e), a three-dimensional network of corner sharing tetrahedral with a sublattice of exchange coupled spins occurs in the oxide pyrochlore family. The sublattice of each of the two metal ions (A and B) form infinite, interpenetrating, networks of such corner-sharing tetrahedra.

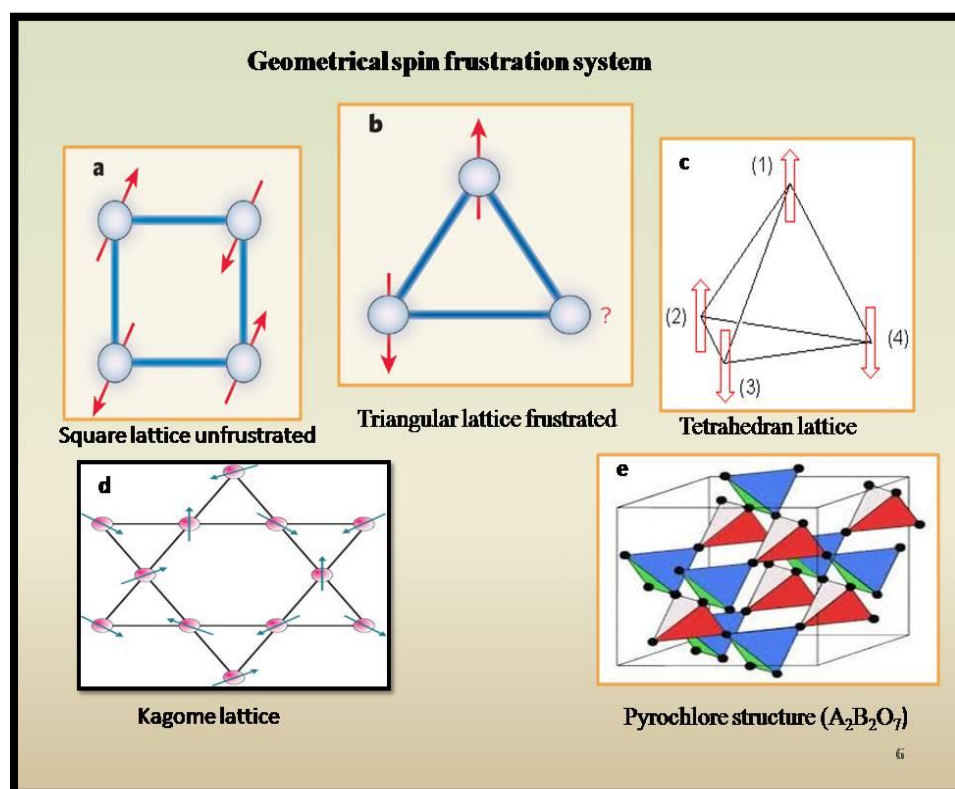


Fig.1.1. Schematic illustrations of geometrical spin frustrated system; (a) Square lattice unfrustrated (b) Triangular lattice frustrated system (c) Tetrahedron lattice frustrated system (d) Two dimensional section of kagome lattice (e) Three dimensional Pyrochlore structure.

Geometrical spin frustration has been recognized to be one of the candidates for the magneto electric multiferroic materials. The frustrated system, exhibiting to the vast degeneracy arising from competing magnetic interactions, generally displays complex magnetic orders at low temperatures like noncentrosymmetric, noncollinear magnetic orders. These exotic magnetic structures sometimes break the

crystal symmetry and can be an origin of the ferroelectricity. Below we present a brief review on different phenomena observed in the frustrated systems and on the studies of Delafossites CuFeO_2 , CuCrO_2 and Crednerite CuMnO_2 .

1.1 .1 Griffith phase:

In the Griffith phase model, a system of diluted Ising ferromagnets in which below a characteristic temperature (T_G), finite size clusters of ferromagnetically correlated spins exist until long range ordering temperature (T_C) and remain distributed in a paramagnetic (PM) matrix. The temperature range between T_C and T_G corresponds to a Griffith phase, and this is different from the paramagnetic as well as the long-range FM phase. In magnetic systems, it was shown that the observation of a Griffiths phase (GP) may have many different origins, *e.g.*, phase separation, competing intra- and interlayer magnetic interaction, occurrence of clusters of sizes ranging from nanometers to micrometers, *etc.*

A Karmakar et.al.[1] (2013) have reported a Griffiths-like phase in isovalent doped rare-earth manganites $\text{R}_{0.5}\text{Eu}_{0.5}\text{MnO}_3$ ($\text{R} = \text{Pr}, \text{Nd}, \text{Sm}$). The dc and ac magnetic studies demonstrate aspects of Griffiths phase-like behaviour. The presence of short range ferromagnetically correlated spin clusters is observed above the antiferromagnetic transition temperature. Rietveld refinement of the structural data reveals strong orthorhombic and Jahn–Teller distortions. In this case presence of only Mn^{3+} and the absence of ferromagnetic double-exchange interaction, only superexchange interactions prevail in such cases which may be both FM and antiferromagnetic. The presence of Mn^{3+} sets up a dominant Jahn–Teller effect which produces enormous structural disorder through bending of Mn–O–Mn bond angles and deformation of Mn–O bond lengths. This may also lead to various magnetic phase separations. Among them, preformation of FM clusters much above the long range ordering temperature (T_C) or the appearance of a Griffiths phase have been the subject of much attention in recent times. Griffiths considered a system of diluted Ising ferromagnets and showed that below a characteristic temperature (T_G), finite size clusters of ferromagnetically correlated spins exist until T_C and remain distributed in a paramagnetic matrix. They showed the family of half isovalent doped AFM $\text{R}_{0.5}\text{Eu}_{0.5}\text{MnO}_3$ ($\text{R} = \text{La}, \text{Pr}, \text{Nd}, \text{Sm}$) exhibits similar GP-like behaviour.

Nicolas Perez et.al. [2] (2013) have reported Griffiths-like phase and magnetic correlations at high fields in Gd_5Ge_4 . Ac susceptibility measurements as functions of temperature at several dc fields and frequencies show the existence of ferromagnetic and antiferromagnetic correlations in the paramagnetic region, where a Griffiths-like phase appears below ~ 225 K. Griffiths-like phase is associated with an effective critical slowing down. On the other hand, high field magnetization measurements reveal the presence of FM and AFM correlations in the three magnetic phases such as PM, FM, and AFM, giving rise to a variety of mixed magnetic states. They study the GL phase by means of ac susceptibility at several low-dc fields and frequencies. They showed that the GL phase takes place in the PM region, yielding an effective critical slowing down associated with competing AFM and FM magnetic correlations. Moreover, the FM correlations extend all the way into the AFM phase. They also report new competing effects from measurements at high magnetic fields, in the vicinity of the first-order magnetostructural transition, in which AFM correlations are retained in the main FM phase. The dependence on frequency of χ' the GL phase is shown, steady decay without any maxima is observed in the frequency range 0.1 to 1 kHz and increase of the slope is noticeable at the onset of the GL anomaly between 228 and 225 K. As the frequency increases, a reduction of the signal in both χ' and χ'' and a slight shift of the anomaly to higher temperatures. The dynamics of critical phenomena in correlated and noncorrelated systems is characterized by the shift of the critical temperature per frequency decade. This is expressed as $\frac{\Delta T_G}{T_G \log \omega}$ where ω is the ac frequency.

J. Albillos et.al. [3] (2009) have studied Griffiths-like phase in the paramagnetic regime of $ErCo_2$. Several characteristics shared by systems showing a Griffiths phase are present in $ErCo_2$, namely the formation of ferromagnetic clusters in the disordered phase, the loss of analyticity of the magnetic susceptibility and its extreme sensitivity to an applied magnetic field. The Griffiths-like phase is then the region between the completely ordered state and the conventional disordered paramagnetic state. They have measured ac magnetic susceptibility as a function of temperature $\chi_{ac}(T)$ and as a function of excitation frequency ω , $\chi_{ac}(\omega)$ in a variety of polycrystalline $ErCo_2$ samples. Magnetic ac susceptibility measurements as a function of temperature and

excitation frequency have been performed in order to study the dynamic properties of the ErCo₂ paramagnetic phase. The $\chi_{ac}(T)$ measurements show the expected Curie–Weiss dependence coming from the Er independent moments. They have studied the dependence of that anomaly with the temperature, the applied magnetic field and the excitation frequency, showing that a relaxation process occurs in the Co sublattice.

Krishanu Ghosh et.al. [4] (2009) have showed Griffiths phase behaviour in a frustrated antiferromagnetic intermetallic compound. The rare coexistence of a Griffiths phase and a geometrically frustrated antiferromagnetism in the non-stoichiometric intermetallic compound GdFe_{0.17}Sn₂. Antiferromagnetic compounds which show characteristic reminiscent of a GP the paramagnetic Weiss temperature is found to be positive, suggesting the presence of strong FM interactions. The only GP compound is an Ca₃CoMnO₆ that exhibits negative θ_p . Most of the GP compounds the FM interactions compete quite strongly with dominant AFM interaction, resulting in positive θ_p . The negative value of θ_p (– 59 K), estimated from inverse magnetic susceptibility in the paramagnetic region and the absence of spontaneous magnetization in the Arrott plot, M^2 vs. H/M suggest that GdFe_{0.17}Sn₂ orders antiferromagnetically at $T_N \sim 16.5$ K. The isothermal magnetizations measured below T_N , do not exhibit any hysteresis behaviour and have a near linear magnetic field dependence. In the GP model, the long-range ordering temperature, $T_C(x)$, of a randomly diluted ferromagnet will be lower than the same of the undiluted one (T_C). The thermodynamic properties will be non-analytical in this region $T(x) < T < T_{undiluted}$ due to the formation of a low density clusters with short-range ordering. Here $T_{C,undiluted}$ is the temperature at which this GP forms and is popularly known as the Griffiths temperature (T_G). The temperature range between T_C and T_G corresponds to a GP, and this GP is different from the paramagnetic as well as the long-range FM phase. χ^{-1} in such case should generally follow power law behaviour describing the Griffith singularity $\chi^{-1} \propto (T - T_C^R)^{1-\lambda}$ where λ is the magnetic susceptibility exponent, and T_C^R is the critical temperature of random ferromagnetic clusters where susceptibility tend to diverge.

1.1 .2 Spin Glass:

In class of spin glass system, the magnetic moments exist in frozen random arrangements. Its state was defined as a random, mixed-interacting magnetic system characterized by a random, cooperative, freezing of spins at a well defined temperature T_f below this temperature, it shows highly irreversible, metastable frozen state without the usual magnetic long range ordering. The frequency dependent data, described by conventional critical slowing down $\tau = \tau_0 \left(\frac{T_f - T_{SG}}{T_{SG}} \right)^{-z\nu'}$ here, T_{SG} is the spin glass transition temperature and T_f is the frequency-dependent freezing temperature at which the maximum relaxation time τ of the system corresponds to the measured frequency. In order to confirm spin glass behavior, generally temperature dependent dc magnetization with different fields, frequency and field dependent ac susceptibility, and isothermal remanent magnetization measurements are carried out.

S. Chatterjee et. al.[5] (2002) have investigated structural, magnetic, and electrical properties of $Y_{0.5}Sr_{0.5}MnO_3$ and $Y_{0.4}Sr_{0.6}MnO_3$. Magnetic study e.g., the frequency dependence of ac susceptibility, zero-field-cooled and field-cooled magnetization behavior, $M(H)$ behavior indicate the spin-glass-like behavior in these materials. Magnetization has a bifurcation between ZFC and FC data at an irreversibility temperature T_{irr} . The $M(H)$ curves show no saturation upto the magnetic field 5 T. It was found that at low field magnetization data follow de Almeida–Thouless line. Electrical resistivity data shows insulating behavior at spin-glass state and do not change with the application of a 4 T magnetic field.

S. Lin et.al. [6] (2009) have studied, structure, and magnetic and electrical/thermal transport properties of a Cr-based antiperovskite compound $PdNCr_3$. It was observed that in temperature dependent magnetization $M(T)$ under ZFC and FC processes and inverse susceptibility (FC) curves of $PdNCr_3$ at a magnetic field of 1 kOe between 5 and 300 K a weak irreversibility between $M_{ZFC}(T)$ and $M_{FC}(T)$ curves below $T_{dif} = 72$ K (defined by the temperature where $M_{ZFC} = M_{FC}$) and a sharp cusp in $M_{ZFC}(T)$ curve around $T_p = 48$ K (defined by the maximum value of magnetization after ZFC process), which are indications of spin glass transition. It was observed that, temperature dependence of dc magnetization $M(T)$ after ZFC and FC at different magnetic fields, magnetization increases with increasing magnetic field, while the T_p shifts to lower temperatures with increasing magnetic field, indicating the frozen spin

glass state. Real part of ac susceptibility as a function of temperature, ac field of $H_{ac} = 3$ Oe with several fixed frequencies $f = 1, 10, 100, \text{ and } 1000$ Hz. It was found that the ac susceptibility exhibits a strongly frequency-dependent peak. As the frequency increases, the sharp peak shifts to higher temperatures, while the magnitude decreases, suggesting a characteristic feature of typical spin glass behavior with a freezing temperature $T_f = 64$ K. A criterion often used to compare the frequency dependence of freezing temperature T_f in different SG systems is to compare the relative shift in freezing temperature per decade of frequency: $\delta F = \frac{\delta T_f}{T_f \Delta(\log 10f)}$. For PdNCr₃, they found that $dT_f = 0.0156$, which is intermediate between those reported for the metallic SG systems, $dT_f = 0.005$ for CuMn alloy and those reported for noninteracting ideal superparamagnetic systems, $dT_f = 0.1$ for isolated particles theory.

D. N. H. Nam et. al. [7](2013) have studied dynamic magnetic properties of La_{0.95}Sr_{0.05}CoO₃ perovskite evidence the existence of a low-temperature spin-glass phase. Dynamic scaling analysis of ac susceptibility data according to conventional critical slowing down implies a finite spin-glass phase-transition temperature $T_g \sim 14.6$ K and a dynamic exponent $z\nu \sim 10.3$. Time relaxation and aging effects were observed at all temperatures in the spin-glass phase. Also temperature cycling experiments, La_{0.95}Sr_{0.05}CoO₃ has a low-temperature spin-glass phase. The existence of a spin-glass phase evidences disorder and frustration i.e., there is a random distribution of ferromagnetic and antiferromagnetic interaction in the system.

1.1.3 Magnetoelectric effect:

Magnetoelectric materials having ferroelectric and magnetic order simultaneously, but also display coupling between these properties. The coupling between (ferro)electric and magnetic order is called the magnetoelectric effect and is defined as the induction of magnetization by an electric field or the induction of electric polarization by a magnetic field.

H. Arkenbout. et.al. [8] (2006) have investigated that ferroelectricity in the cycloidal spiral magnetic phase of MnWO₄ and the relationships among magnetic, dielectric, and ferroelectric properties of a frustrated spin system MnWO₄, which undergoes several magnetic phase transitions including a commensurate

,incommensurate and a collinear-noncollinear transition. They have measured dielectric and pyroelectric measurements show that the transition into a spiral magnetic ordered phase produces a ferroelectric state. The direction of the electric polarization is perpendicular to the spin rotation axis and the propagation vector of the spiral. The geometrical relation between the proposed magnetic structure and the direction of the electric polarization observed in the current study agrees well with the prediction of recent theoretical studies on the ferroelectricity in cycloidal spiral magnetic systems. They suggests that MnWO_4 is a new member in the family of the multiferroic systems, in which the cycloidal spiral magnetic order induces a ferroelectric order. The shift of phase boundaries, induced by magnetic fields, depends on the difference in the net magnetization between the ferroelectric phase and neighboring paraelectric phases.

S. Chowki et.al. [9] (2014) have observed electric polarization in the magnetically ordered state of the Haldane chain compound, $\text{Gd}_2\text{BaNiO}_5$, with strongly correlated magnetic and dielectric properties. They have performed results of dc magnetic susceptibility and heat capacity measurements indicate two magnetic transitions, one corresponding to the anti-ferromagnetic order at $T_N \sim 55\text{K}$ and the other to spin-reorientation transition at $T_{SR} \sim 24\text{K}$. The dielectric permittivity ϵ'_r and loss $\text{Tan}(\delta)$ also exhibit anomalies in the vicinity and T_N , respectively. Another interesting finding is that $\Delta\epsilon'_r = (\epsilon'_r(H) - \epsilon'_r(0))/\epsilon'_r(0)$ changes its sign at the critical magnetic field. The origin of the observed magneto-electric effect is discussed on the basis of spin-phonon coupling. Raman and infrared spectroscopy studies also establish the strong correlation of magnetic excitations with lattice dynamics. The frequency and half width of the observed phonon modes exhibit pronounced temperature dependence peaking at T_N .

Tathamay Basu. [10] (2015) have studied magnetic and magnetodielectric behavior of GdCrTiO_5 . They have carried out dc magnetization, heat-capacity, and dielectric studies down to 2K for the compound GdCrTiO_5 , crystallizing in orthorhombic $Pbnm$ structure, in which well-known multiferroics RMn_2O_5 , R=Rare-earths. The magnetic ordering temperature of Cr appears to be suppressed compared with that in isostructural Nd counterpart, NdCrTiO_5 . This finding on the Gd

compound suggests that Nd 4f hybridization plays an uncommon role in the magnetism of Cr. Dielectric constant does not exhibit any notable feature below about 30K in the absence of external magnetic field, but a peak appears and gets stronger with the application of external magnetic fields, supporting the existence of magnetodielectric coupling. The dielectric anomalies appear even near 100K, which can be attributed to short-range magnetic-order. They have also measured Raman spectra in the frequency range 150–400 cm^{-1} supporting short-range magnetic order. They have investigated magnetic and magnetodielectric behaviour of a new member in another family RCrTiO_5 that belongs to the same structure as the wellknown magnetoelectric system, RMn_2O_5 , in which geometrical frustration plays a role on multiferrocity.

Y. Fang [11] (2014) have performed, magnetic and electric measurements. Pyroelectric current was collected using an electrometer (Keithley 6514A) after poling the sample in an electric field. In detail, the sample was first submitted to the PPMS and cooled down to 70 K. Then a poling electric field of 667 kV/m was applied on the sample with temperature decreasing from 70 to 10 K. In order to release any charges accumulated on the sample surfaces or inside the sample, the sample was short circuited for long-enough time. During the recording of pyroelectric current, the sample was heated slowly at a warming rate of 3 K/min. Magnetic field was applied throughout the cooling and warming processes. Magnetic properties (SQUID) magnetometer with applied magnetic fields. It concludes that they have performed detail measurements on ME properties of polycrystalline $\text{Co}_4\text{Nb}_2\text{O}_9$. The experimental results reveal that no spontaneous polarization arises below T_N unless a high enough magnetic field is applied. The polarization increases proportionally with the applied magnetic field, showing a linear ME effects.

1.1.4 Delafossite and Crednerite structure:

Delafossite was first noted by *Charles Friedel* in 1873 and given the composition $\text{Cu}_2\text{O}_3.\text{Fe}_2\text{O}_3$. The mineral was given the name delafossite in honor of the French mineralogist and crystallographer *Gabriel Delafosse* (1796–1878). The delafossite structure can be visualized as consisting of two alternate layers: a planar layer of A cation in a triangular pattern and a layer of edge-sharing BO_6 octahedra flattened with

respect to the c -axis. Depending on the orientation of each layer in stacking, two crystalline forms are shown in figure 1. As shown in figure 1(a), by stacking the double layers with alternate A layers oriented 180° relative to each other, the hexagonal 2H type is formed which has $P63/mmc$ space group symmetry. If the double layers are stacked with the A layers oriented in the same direction relative to one another but offset from each other in a three layer sequence, the rhombohedral 3R type is formed that has the space group symmetry of $R3m$, which is shown in figure 1(b). The standard delafossite crystal structure is rhombohedral $R\bar{3}m$ such as in CuCrO_2 or CuFeO_2 , and the magnetic lattice is a stacking of perfect triangular arrays. Though related to the delafossite structure, crednerite CuMnO_2 is not rhombohedral at room temperature (RT): in CuMnO_2 , the Jahn-Teller (JT) distortion of the $\text{Mn}^{+3}t_{2g}^3e_g^1$ cation lifts the e_g orbitals degeneracy thus leading to a distorted monoclinic structure, $C2/m$, at room temperature. In particular, CuFeO_2 and CuCrO_2 have been extensively studied in terms of magnetoelastic coupling and magnetoelectric multiferroics, which are considered to be associated with spin frustration.

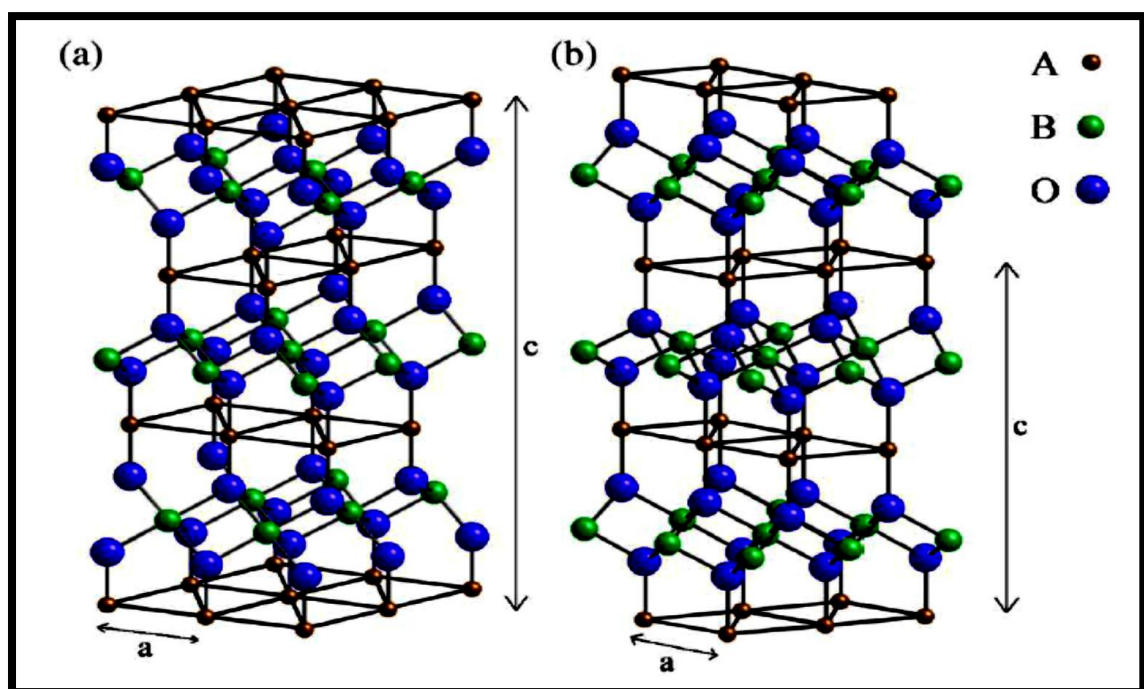


Fig.1.2. Delafossite crystal structure: (a) Hexagonal structure and (b) Rhombohedral structure. (Courtesy: Da Li et al; J. Phys. D, Appl. Phys. 49:10–15, 2007)[12]

1.1.4.1 CuCrO₂:

In the delafossite structure (space group $R\bar{3}m$), Cr³⁺ ions ($S = 3/2$) form triangular-lattice planes stacked along the hexagonal c axis. On the triangular-lattice planes, spin frustration arises, and then the screw spiral magnetic structure having the degree of freedom of spin chirality is stabilized to release the spin frustration. On the triangular-lattice planes, spin frustration arises, and then the screw spiral magnetic structure having the degree of freedom of spin chirality is stabilized to release the spin frustration. The ferroelectricity accompanied by the screw spiral order in CuCrO₂ is reasonably explained by the so-called p - d hybridization model, in which electric polarization induced by a spin-dependent orbital hybridization between $3d$ (metal) and $2p$ (ligand) does not cancel out in a crystal when the crystal possesses relatively lower crystal symmetry.

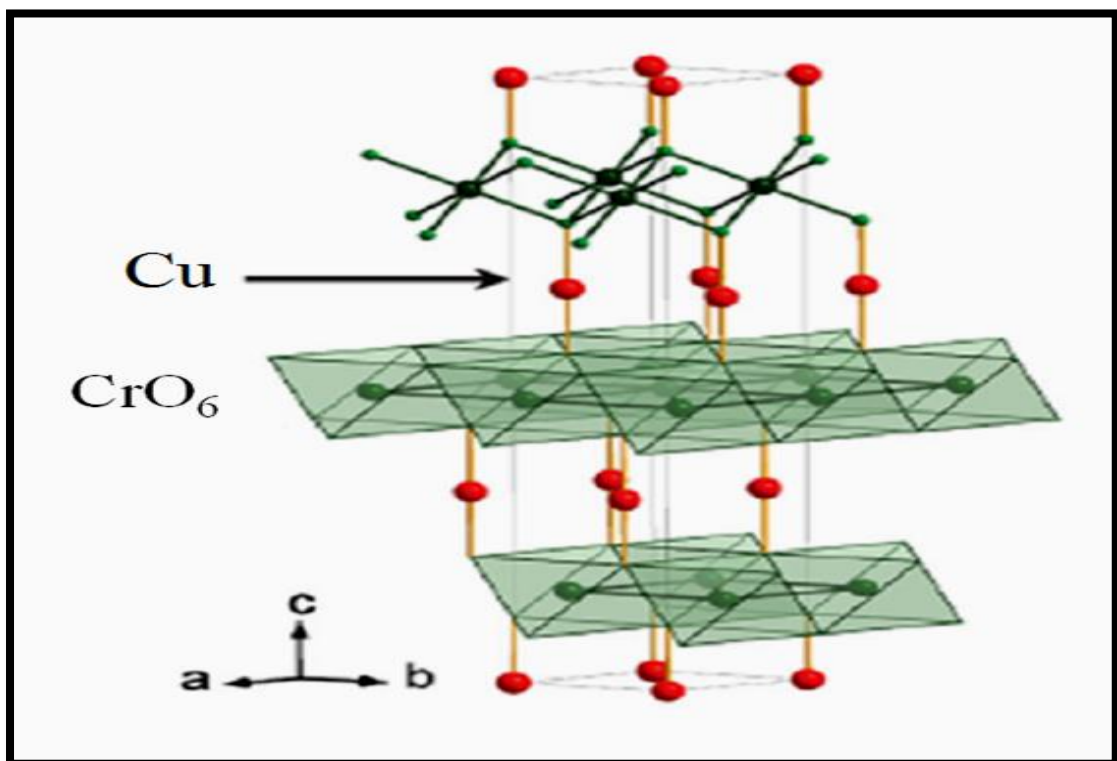


Fig.1.3. Crystal structure of Delafossite CuCrO₂. (Courtesy: E. Pachoud et.al, Phys Rev B 86, 054437 (2012)[13])

K. Kimura, et.al.[14] (2009) have investigated magnetic, ferroelectric, and magnetoelectric properties of a triangular lattice antiferromagnet, CuCrO₂, with the

out-of-plane 120° spin structure. They observed a first-order magnetoelectric phase transition induced by magnetic fields applied along the (1-10) direction. They found that ferroelectric polarization reversal can be tuned by using both magnetic and electric fields in the triangular lattice antiferromagnet. CuCrO_2 exhibit an extremely low electric coercive field for the ferroelectric polarization reversal in the absence of magnetic fields among magnetically induced ferroelectrics. The electric coercive field is highly sensitive to the external magnetic field, which enables the polarization reversal by magnetic fields. It was observed that the coercive magnetic field for the polarization reversal can be tuned by the electric field, implying that the electric field can change the magnetic property in CuCrO_2 .

Eundeok Mun et.al.[15] (2009) have studied different types of spiral magnetic orderings that can form spontaneously due to frustration in triangular-lattice antiferromagnets. It was monitored that the magnetic phase diagram up to 65 T along all the principal axes, and also use electric polarization to probe changes in the spiral order at high magnetic fields. The $H - T$ phase diagram of single-crystalline CuCrO_2 is explored up to 60 T in magnetization and 65 T in electric polarization for all the principal directions of P and H . At lower temperatures, the magnetic structure undergoes a stretching through incommensurate and commensurate wave vector. It was observed that the previously reported spin-flop transition to a cycloidal-spiral magnetic phase near 5.3 T, and find that it is insensitive to temperatures between 1.6 K and the ordering temperature at $T_{\text{MF}} = 23.6$ K. CuCrO_2 shows strong magnetic frustration due to its triangular spin configuration in the ab plane, and evidenced by the discrepancy between the 24 K 2D ordering temperature and the 270 T saturation magnetization and 200 K Curie-Weiss temperature. It was observed that multiple magnetic and ferroelectric phases accessibly by relatively small magnetic fields relative to the saturation magnetic field. However, within most of the phases, there is almost no obvious variation of the electric polarization with magnetic field. This may be due to the fact that in most cases of magnetically induced electric polarization, the leading behavior of P is M^2 , and so P will show most of its magnetic field dependence at higher magnetic fields. CuCrO_2 is a frustrated magnet with a rich variety of magnetic and ferroelectric phases that couple to each other and extend beyond 65 T.

O. Aktas *et.al.*[16] (2013) have studied the magnetic phase diagram of the multiferroic geometrically frustrated antiferromagnet CuCrO_2 determined using dielectric constant and ultrasonic velocity measurements with the magnetic field parallel to the [1-10] direction. It was observed that, at zero field the magnetoelectric phase induced by a proper screw magnetic ordering is obtained below $T_{N1} = 23.4$ K, while the velocity measurements reveal another transition at $T_{N2} = 24.3$ K. As the dielectric and velocity measurements were performed simultaneously which confirms the presence of an intermediate nonferroelectric magnetic state between the magnetoelectric and paramagnetic phases. They have also studied detailed analysis of the elastic properties of CuCrO_2 . Analysis of the data using a Landau-type free energy indicates that CuCrO_2 undergoes a first-order pseudoproper ferroelastic transition leading to a $-3m-2/m$ structural transition at T_{N2} . The order parameter of the ferroelastic-antiferromagnetic transition at T_{N2} belongs to the E_g irreducible representation of the trigonal $3m$ point group, and the magnetic moments must act as a secondary order parameter.

Takuya Aoyama *et.al.*[17] (2013) have reported, effects of pressure on crystallographic structure, magnetism, and spin-driven ferroelectricity in the delafossite CuCrO_2 . They have successfully established a measurement system which allows dielectric, ferroelectric, and ac calorimetric measurements under high-pressure conditions by using a diamond anvil cell. They investigated pressure effects on the structure and magnetoelectric properties of a multiferroic triangular-lattice antiferromagnet, CuCrO_2 . It was found that the magnetic transition temperature into the spin-spiral ferroelectric ordered phase T_N significantly increases with pressurization. However, the magnitude of the dielectric anomaly at T_N is suppressed by applying pressure, and the magnitude of the spontaneous polarization below T_N is abruptly suppressed at around 8 GPa. These results suggest that a ferroelectric-antiferroelectric transition has occurred as the Cr-layer spacing becomes shorter and the interlayer exchange integral becomes larger with pressurization. The coercive field for the polarization reversal becomes large with pressurization, which can be interpreted in terms of the magnetoelectric domain rearrangement. This result clearly

demonstrate that the application of pressure can be an effective perturbation in the investigation and tuning of magnetoelectric properties in multiferroic materials.

Kenta Kimura *et.al.*[18] (2013) have performed magnetic and dielectric properties of CuCrO_2 single crystals. They found that CuCrO_2 undergoes two successive magnetic phase transitions, probably into a collinear antiferromagnetic structure and then the out-of-plane 120° spin structure. Ferroelectricity appears in the out-of-plane 120° spin phase where the spin chirality develops, indicating the spin chirality can be detected and controlled through magnetoelectric coupling. It was observed that the out-of-plane 120° spin structure provide an opportunity for a unique control of spin chiral ferroelectric domain structures by using electric and/or magnetic fields. Two magnetic phase transitions are observed at $T_{N2} \sim 24.2$ K and $T_{N1} \sim 23.6$ K. It was found that ferroelectric polarization along the triangular lattice plane develops at T_{N1} , suggesting that the system undergoes a transition into an out-of-plane 120° spin-chiral phase at T_{N1} . One of the most typical frustrated magnetic structures is a 120° spin structure in a triangular lattice antiferromagnet in which three spins form 120° angles with neighboring spins. This spin structure is the most ideal object to investigate the magnetoelectric correlation because of its simple commensurate spiral structure. Two types of the 120° spin structures appear on TLA, depending on the sign of single-ion anisotropy D , with $D > 0$ (easy-plane type), a 120° structure whose spin spiral plane is parallel to the triangular lattice plane emerges (in-plane 120° structure), whereas in the case of $D < 0$ (easy-axis type), a 120° structure whose spiral plane is normal to the TLP shows up (out-of-plane 120° structure).

M. Poienar *et.al.*[19] (2010) have investigated the magnetic couplings stabilizing of the magnetic structure of CuCrO_2 . Spin dynamics of the geometrically frustrated triangular antiferromagnet multiferroic CuCrO_2 has been mapped out using inelastic neutron scattering. They have determined the relevant spin Hamiltonian parameters which features that the helicoidal model with a strong planar anisotropy correctly describes the spin dynamics. In order to study the different magnetic interactions stabilizing this helicoidal structure. Inelastic Neutron scattering experiments was carried out on a single crystal of CuCrO_2 . They have performed energy calculations based on a standard Heisenberg model to determine the $(J_{ab}, J'_{ab}, J_{NN}, J_C)$ phase

diagram of the classical ground state of CuCrO_2 and to investigate the influence of $\frac{J'_{ab}}{J_{ab}}$, J_{NN} , and J_c on the incommensurate deviation away from the classical 120° structure.

Qinggang Meng *et.al.*[20] (2010) have reported Mg doped CuCrO_2 samples. It was observed that thermoelectric properties of sol gel prepared samples improved over bulk samples. The substitution of Mg could give four orders improvement on electrical conductivity up to 10.34 S/cm at room temperature compared with the undoped samples. The positive Seebeck coefficients of doping oxides implied the typical p-type conducting oxides by sol–gel method. The highest value of power factor has been achieved to be $1.37 \times 10^{-4} \text{ W m}^{-1} \text{ K}^{-2}$ for $\text{CuCr}_{0.90}\text{Mg}_{0.10}\text{O}_2$ at 470 K.

Kiran Singh *et.al.*[21] (2010) have performed dielectric susceptibility and spin glass properties of polycrystalline $\text{CuCr}_{0.5}\text{V}_{0.5}\text{O}_2$. Electron diffraction, high resolution electron microscopy and electron energy loss spectroscopy show that the Cr^{3+} and V^{3+} magnetic cations are randomly distributed on the triangular network of CdI_2 -type layers. They also showed that CuCrO_2 , $\text{CuCr}_{0.5}\text{V}_{0.5}\text{O}_2$ exhibits two distinctive (magnetic and electric) glassy states evidenced by memory effects in electric and magnetic susceptibilities. A large magnetodielectric coupling is observed at low temperature.

M. Frontzek *et.al.*[22] (2010) have studied the multiferroic CuCrO_2 by means of single crystal neutron diffraction. They observed the two close magnetic phase transitions at $T_N = 24 \text{ K}$ and $T_{mf} = 23 \text{ K}$. Analysis shows that the low temperature magnetic ordering of CuCrO_2 is fully three-dimensional and can be described as an incommensurate proper helix propagating in the $[\text{H};\text{H}; 0]$ direction. Why is CuCrO_2 not multiferroic between T_N and T_{mf} ? According to the *Arima* model, the in-plane proper screw spiral will create a spontaneous polarization even without the observed three-dimensional order. The propagation vector in the narrow phase is the same as in the multiferroic phase. In this case, two-dimensional nature this narrow phase has been discussed as a possible collinear state. The result shows that propagation vector remains the same in both phases. In combination with the absence of a net

ferromagnetic component and the continuous course of the susceptibility through the transition at T_{mf} , this indicates that spirals already form at T_N .

Phillip T Barton *et al.*[23] (2012) have studied delafossite diamagnetic $CuAlO_2$ and frustrated antiferromagnet $CuCrO_2$. Neutron diffraction studies have been essential in explaining the magnetism and multiferroic behavior of $CuCrO_2$. The first neutron study by *Kadowaki et al* revealed that $CuCrO_2$ has an antiferromagnetic out-of-plane 120 spin structure and short correlation length along the c axis. Further study by *Poienar et al* narrowed the magnetic structure possibilities to either helicoidal or cycloidal, and investigated the effect of Mg substitution. *Soda et al* confirmed a noncollinear helicoidal magnetic structure through triple-axis spin-polarized neutron scattering experiments on a single crystal. Such a magnetic structure also occurs for $CuFeO_2$ under an applied magnetic field or with Al substitution, was found to give rise to ferroelectricity. This is consistent with a theoretical model proposed by *Arima*, which shows that a noncollinear helical spin structure and spin-orbit coupling give rise to the multiferroic behavior. In the case of $CuCrO_2$, the presence of two magnetic transitions in $CuCrO_2$ was revealed by a careful further examination of a single crystal. $CuCrO_2$ included inelastic neutron scattering to map out the spin dynamics of the system. The results are consistent with the work of Kimura et al, critical role of next-nearest-neighbor exchange interactions in stabilizing magnetic order. XRD and magnetic study can be explained by magnetic frustration and chemical disorder. It demonstrates that the understanding magnetic frustration and for the tuning of physical properties through chemical substitution.

Shijun Luo *et al.*[24] (2012) have studied multiferrocity behavior of Ni doped in $CuCrO_2$. It was found that ferromagnetism and ferroelectricity enhanced in $CuCrO_2$ -based multiferroics. They performed multiferroic characterization ferroelectricity using the pyroelectric current method integrated with the Quantum Design Physical Properties Measurement System. To obtain the $T(H)$ dependence of P , the pyroelectric current was collected at a 4 K/min T -sweeping rate (0.6 T/min H -sweeping rate). At the optimized doping level $x=0.05$. It was observed that not only an enhancement of one order of magnitude in magnetization but also a significant increasing of polarization up to $50\mu C/M^2$ from $35\mu C/M^2$ of polycrystalline $CuCrO_2$.

The measured magnetic properties of both CCNO and CCO shows the field-cooling, M as a function of T cooling field $H=500\text{Oe}$. Obviously the measured M for CCNO over the whole T -range (2–300 K) is 10–20 times larger than that for CuCrO_2 , demonstrating a significantly enhanced ferromagnetism with respect to CuCrO_2 .

T. N. M. Ngo *et.al.*[25] (2012) have measured the thermally stimulated depolarization currents of multiferroic CuCrO_2 . They observed a sharp peak near the antiferromagnetic ordering temperature $T_N=24\text{ K}$, below which the material becomes ferroelectric. The pyroelectric effect is of increasing significance for characterizing ferroelectrics. This effect is being used when the measurements of polarization-electric field hysteresis loop are not effective this can be caused by the small electric polarization obtained in improper ferroelectric materials such as multiferroics. They performed PC and thermally stimulated depolarization currents measurements on polycrystalline delafossite CuCrO_2 . The peak current saturates at $\sim 12\text{ pA}$ with a poling field of $\sim 500\text{ kV/m}$. Hence, applying a higher external field to obtain a larger PC peak is unnecessary for determining the spontaneous polarization. Different heating rates of 1, 2, 5, and 10 K/min were used while measuring the peak position to test the effect of heating rate such that the PC peaks shift to higher temperatures for larger heating rates. CuCrO_2 shows in addition to the PC peak at the ferroelectric transition, TSDC peaks when the material is poled at temperatures above T_N . The ferroelectric transition is well defined with a clear sharp peak at $\sim 24\text{ K}$. When the sample is poled at 125 K, three TSDC peaks are observed at $\sim 50, 120, \text{ and } 150\text{ K}$. The peak near 50K is consistent with the defect dipole relaxation as the TSDC increases linearly with the increase of poling fields with a fixed T_m . The second peak near 120K is assigned to space charge relaxation due to the release of trapped charges. TSDC peak at T_m shifts quadratically with the poling field at low temperature. The third peak around 150K is assigned to ionic space charge depolarization. The space charge related origins of the peaks around 120 and 150K are consistent with the observation of Maxwell–Wagner type dielectric relaxation originating from a Schottky barrier formation at the interface between the electrodes and the sample.

1.1.4.2 CuFeO₂:

CuFeO₂ has the characteristic delafossite structure (space group $R\bar{3}m$) with lattice constant $a=3.03 \text{ \AA}$ and $c =17.03 \text{ \AA}$ at room temperature. The structure consists of hexagonal layers of Cu, O, and Fe with a stacking sequence of Cu–O–Fe along the c -axis to form a layered triangular lattice antiferromagnet. Below about 7T, magnetic ground state of CuFeO₂ is collinear 4-sublattice ($\uparrow\uparrow\downarrow\downarrow$) phase. Above 7T, it exhibits multiferroic behavior and is characterized by a complex noncollinear state. At about 13 T, complex non collinear phase transforms into a 5-sublattices phase, which does not exhibit multiferroic behavior possibly because it is commensurate. The 5-sub lattice phase is stable up to about 20 T, above which a canted 3-sublattice phase becomes the ground state. At 34 T, 3-sub lattice phase transform into a conical-type phase. A different conical phase appears at about 50 T. At 70 T, small spins become aligned in which the CL-1 (ferromagnetic) phase. (J. T. Haraldsen et al, Phys Rev B **86**, 024412 (2012))

Noriki Terada et al. [26] (2012) have performed dielectric measurements and neutron diffraction experiments on the delafossite AgFeO₂. A ferroelectric polarization $P \approx 300 \mu\text{C}/\text{M}^2$ was observed in a powder sample, below 9 K. The neutron diffraction data shows magnetostructural phase transitions at $T_{N1} =15 \text{ K}$ and $T_{N2} =19 \text{ K}$. Magnetoelectric multiferroic materials, which possess (anti)ferromagnetism and ferroelectricity in a single phase, have been the subject of intensive research. In such systems, complex magnetic structures stabilized by frustrated exchange interactions between spins break inversion symmetry and induce a ferroelectric polarization. Examples of such materials are TbMnO₃ and CoCr₂O₄ with cycloidal magnetic structures. The induced ferroelectric polarization can be explained in terms of the inverse Dzyaloshinskii-Moriya effect or spin current mechanism represented by $\propto r_{ij} \times (S_i \times S_j)$. Moreover, the delafossite family, CuFeO₂, CuCrO₂ shows ferroelectric polarization induced by the proper screw helical magnetic ordering r_{ij} parallel to the $(S_i \times S_j)$. The magnetic field-induced ferroelectricity in CuFeO₂ has been explained by *Arima* as a combined effect of d-p hybridization and spin-orbit coupling respectively.

Taro Nakajima *et al.*[27] (2012) have performed inelastic neutron scattering measurements in the ferroelectric noncollinear-magnetic phase of $\text{CuFe}_{1-x}\text{Ga}_x\text{O}_2$ with $x = 0.035$ under applied uniaxial pressure. This system has three types of magnetic domains with three different orientations reflecting the trigonal symmetry of the crystal structure by applying a uniaxial pressure of 10 MPa onto the [1-10] surfaces of the single-crystal CFGO sample. They have produced a nearly single-domain multiferroic phase. They have refined the Hamiltonian parameters so as to simultaneously reproduce both of the observed single-domain and multi-domain spectra. Comparing the refined Hamiltonian parameters in the multiferroic phase with those in the collinear 4SL magnetic ground state of undoped CuFeO_2 , they reported that the single-ion uniaxial anisotropy D is significantly reduced and the lattice distortion parameter K is slightly reduced by the nonmagnetic substitution.

Shojan P. Pavunny *et al.*[28] (2010) have investigated by employing X-ray diffraction, X-ray photoemission spectroscopy, energy dispersive X-ray spectroscopy, and scanning electron microscopy. XPS study demonstrated, two Cu $2p_{3/2}$ and $2p_{1/2}$ peaks at 932.5 and 952 eV and two Fe $2p_{3/2}$ and $2p_{1/2}$ peaks at 710 and 725 eV, indicating that Cu and Fe ions are in +1 and +3 states. The valance states of Cu and Fe ions are in +1 and +3 with high spin $S=5/2$ respectively. Room temperature Raman spectra of CuFeO_2 displayed two main Raman active modes at $E_g \sim 351 \text{ cm}^{-1}$ and $A_g \sim 692 \text{ cm}^{-1}$ in accordance with other delafossite structures. The temperature dependent Raman spectra demonstrated, that both the modes shifted to lower frequency with significant decrease in intensity with increase in temperature. Frequency shift and linewidth of both phonon lines matched well with the theoretical damped harmonic oscillator model based on thermal expansion of the lattice and their anharmonicity coupling with other phonons. Lattice dynamic behavior of CuFeO_2 was probed by micro-Raman spectroscopy at ambient cryogenic temperatures.

Chonggui Zhong *et al.*[29] (2010) have studied the origin of ferroelectricity of multiferroic CuFeO_2 with collinear and noncollinear magnetic structure calculations using density functional theory. Comparing the lattice geometry and electronic structures of different magnetic orderings, It was confirmed that the up-up-down-down spin arrangement plays an key role in the formation of band gap, the decrease in

total energy, and the increase in magnetic moment. CuFeO_2 undergoes a large lattice distortion due to helical-spin ordering. In particular, the strong hybridizations of Fe $3d$ with O $2p$ states drive ferroelectric polarization, which provides a first-principle understanding of multiferroicity in CuFeO_2 .

F. Ye, *et al.*[30] (2006) have performed high-resolution synchrotron X-ray and neutron diffraction to study the geometrically frustrated triangular lattice antiferromagnet CuFeO_2 . It was found that CuFeO_2 undergoes two antiferromagnetic phase transitions with incommensurate and commensurate magnetic order at $T_{M1}=14$ K and $T_{M2}=11$ K, respectively. These two magnetic transitions are accompanied by second- and first-order structural phase transitions from hexagonal to monoclinic symmetry. Application of a 6.9 T magnetic field lowers both transition temperatures by ~ 1 K, and induces an additional incommensurate structural modulation in the temperature region where the field-driven ferroelectricity occurs. These results suggest that a strong magneto-elastic coupling is intimately related to the multiferroic effect. Frustrated spin systems have recently attracted considerable attention because of their novel magnetic and multiferroic properties. A strongly frustrated system should exhibit no long-range spin order. However, magnetic frustration can often be lifted by a symmetry-reducing lattice distortion at finite temperature and therefore allow long-range magnetic order at lower temperatures. Similarly, application of a magnetic field can also release the spin frustration and, in some cases, induce electric polarization.

Randy S. Fishman, *et al.* [31](2010) have reported phase diagram of the magnetically frustrated material CuFeO_2 . Monte Carlo simulations, spin wave calculations, and variational techniques provides a powerful and efficient method for evaluating the magnetic phase diagram of a frustrated magnet. For fields $50T < H < 65T$, a new spin-flop phase is predicted between a canted 3-sublattice phase and the conventional conical spin-flop phase. A canted 5-sublattice phase is predicted between the multiferroic phase and either a collinear 5-sublattice phase for pure CuFeO_2 or a canted 3-sublattice phase for Al- or Ga-doped CuFeO_2 .

1.1.4 .3 CuMnO₂:

Crednerite CuMnO₂ having ABO₂-type structure with triangular-lattice antiferromagnet. Unlike other ABO₂-type materials that have B-site cations of Fe³⁺ ($3d^5: t_{2g}^3 e_g^2$) and Cr³⁺ ($3d^3: t_{2g}^3$), the crystal structure of CuMnO₂ does not consist of perfect triangular lattices. It consists of isosceles-triangular lattice which occurs due to Jahn-Teller distortion of Mn³⁺ ($3d^4: t_{2g}^3 e_g^1$) with an orbital degree of freedom. The structural distortions caused by the Jahn-Teller character of the Mn³⁺ and orbital ordering results in the structure with two types of inequivalent Mn-Mn pairs in the MnO₂ plane: those along the *a*-direction with the short Mn-Mn distance of 2.88 Å, while long bonds in two other directions, with the Mn-Mn distance of ~ 3.14 Å as shown in Fig. 2. Exchange coupling in the *ac* plane can be characterized by two exchange constants: J₁ (long Mn-Mn bonds) and J₂ (short Mn-Mn bonds). T < T_N = 65K the structure changes from monoclinic to triclinic C-1 due to magnetostriction.

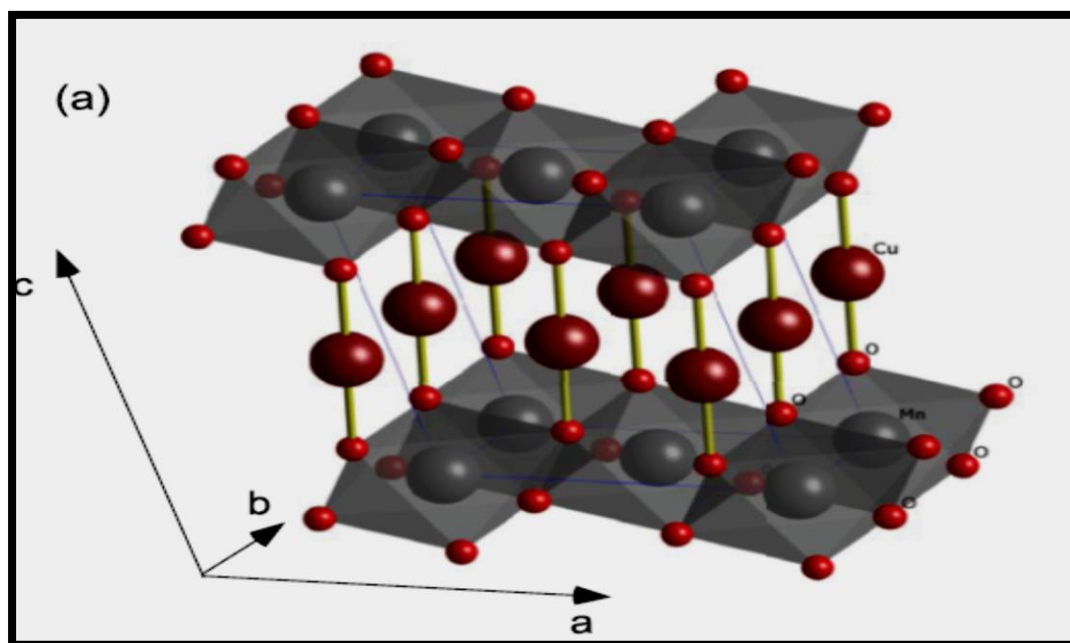


Fig.1.4.Crystal structure of crednerite CuMnO₂ with the monoclinic unit cell.(
Courtesy: Noriki Terada et.al, Phys Rev B,84, 064432, 2011) [32]

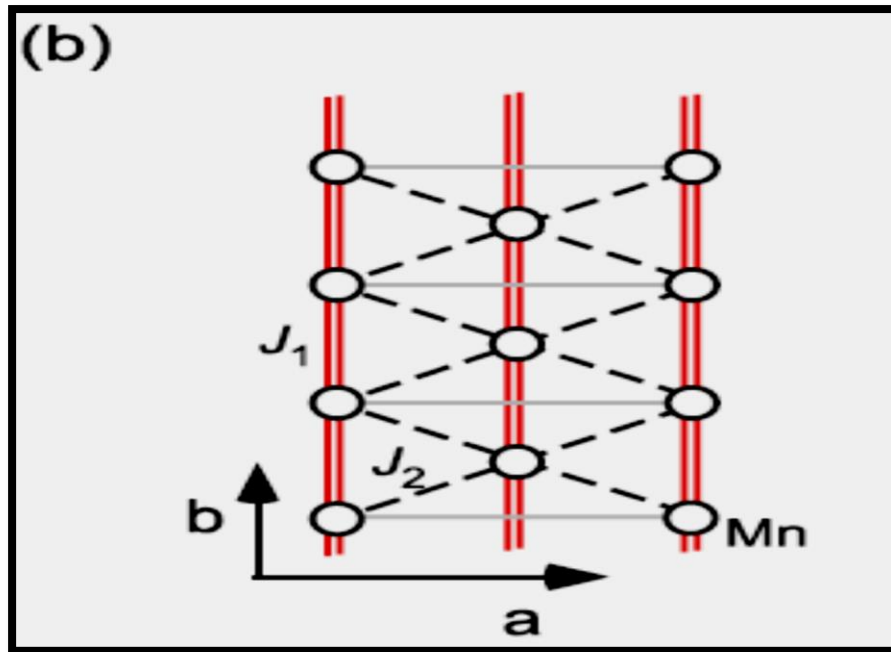


Fig.1.5. Schematic diagram of isosceles triangular lattice layer with the nearest-neighbor and the next-nearest neighbor exchange interactions, J_1 and J_2 . (Courtesy: Noriki Terada et.al, Phys Rev B 84, 064432, 2011) [32]

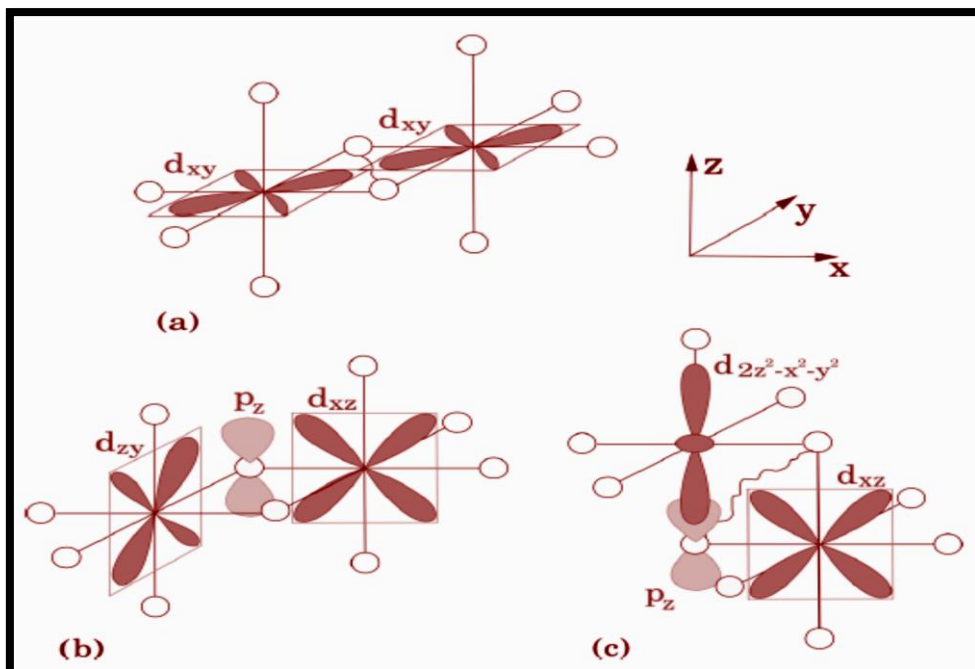


Fig.1.6. Different processes for the exchange coupling of the neighboring Mn^{3+} ions in the MnO_6 octahedra (a) Direct overlap of the t_{2g} orbitals (b) antiferromagnetic t_{2g} - t_{2g} superexchange via oxygen (c) antiferromagnetic t_{2g} - e_g superexchange via oxygen the Jahn-Teller distortion makes the distance between these two Mn ions long. (Courtesy: A. V. Ushakov et.al, Phys Rev B 89, 024406, 2014) [33]

The MnO_6 octahedra in CuMnO_2 , triangular layer have common edge, so that the Mn-O-Mn angle is close to 90° . There exist in this geometry several contributions to the nearest neighbor magnetic coupling. One of them is a direct hopping between the Mn orbitals, especially t_{2g} ones, with the lobes directed towards each other, as shown in Fig.1.6(a). This contribution must be antiferromagnetic. In order to understand the superexchange via O ions, as shown in Fig.1.6(b,c). According to Goodenough-Kanamori-Anderson rules, superexchange between the half-filled t_{2g} orbitals via oxygens will be also antiferromagnetic, $\sim \frac{t_{pd\pi}^4}{\Delta^2} \left(\frac{1}{U} + \frac{2}{2\Delta + U_{pp}} \right)$, where Δ is the charge-transfer energy of the excitation, in our case, $\text{Mn}^{3+} (d^4) \text{O}_2^- (2p^6) \rightarrow \text{Mn}^{2+} (d^5) \text{O}^- (2p^5)$, and U_{pp} is the repulsion of oxygen p electrons. most important contribution to the Mn-Mn exchange via oxygens could be the $t_{2g}-e_g$ exchange, which, for the hopping to the half-filled e_g orbital, is antiferromagnetic, and could be quite strong, $\sim \frac{t_{pd\pi}^2 t_{pd\sigma}^2}{\Delta^2} \left(\frac{1}{U} + \frac{2}{2\Delta + U_{pp}} \right)$.

V. Ushakov et.al.[34] had studied the exchange interactions and magnetic structure in layered system CuMnO_2 and in nonstoichiometric system $\text{Cu}_{1.04}\text{Mn}_{0.96}\text{O}_2$. It comprises triangular layers distorted due to orbital ordering of the Mn^{3+} ions by ab initio band-structure calculations. The exchange interaction parameters for the Heisenberg model within the Mn planes and between the Mn planes are estimated in-plane magnetic structure by direct $d-d$ exchange between neighboring Mn ions. The superexchange via O ions, with 90° , Mn-O-Mn bonds, plays a less important role for the in-plane exchange. The change of interlayer coupling from antiferromagnetic in pure CuMnO_2 to ferromagnetic in doped material is explained. The interlayer coupling is largely dominated by one exchange path between the half-filled $3z^2 - r^2$ orbitals of Mn^{3+} .

C. Vecchini et.al.[35] have reported a detailed analysis of the structural phase transition below the AFM order $T_N = 65$ K in CuMnO_2 by high-resolution neutron powder diffraction. Temperature dependence of the magnetic order parameter and relevant structural parameters, such as cell constants and atomic positions, and analysis of the Landau potential show that there is a unique critical temperature, as

well as that the primary order parameter is magnetic. The structural phase transition, which is essential to lift the magnetic degeneracy, is improper ferroelastic with a linear-quadratic coupling between strain and magnetization density.

M. Poienar et.al.[36] have reported substitution effect on the interplane coupling in crednerite: $\text{Cu}_{1.04}\text{Mn}_{0.96}\text{O}_2$ system. 4%Cu for Mn substitution in CuMnO_2 decreases slightly the lattice parameters, reduces the Jahn-Teller distortion of the MnO_6 octahedra, but does not change the temperature dependence of the structure, exhibiting a $C2/m$ to $P-1$ structural transition. The antiferromagnetic structure is strongly modified by the substitution, as a propagation vector $k=(0, 1/2, 0)$ is supported for $\text{Cu}_{1.04}\text{Mn}_{0.96}\text{O}_2$ as compared to $k=(0, 1/2, 1/2)$ for CuMnO_2 . Synchrotron and Neutron powder diffraction studies of $\text{Cu}_{1.04}\text{Mn}_{0.96}\text{O}_2$ show that the partial Cu for Mn substitution affects mainly the sign of the interplane magnetic coupling that changes from antiferromagnetic in CuMnO_2 to ferromagnetic in $\text{Cu}_{1.04}\text{Mn}_{0.96}\text{O}_2$.

V. Ovidiu Garlea et.al.[37](2011) have studied anisotropic triangular lattice of the crednerite system $\text{Cu}(\text{Mn}_{1-x}\text{Cu}_x)\text{O}_2$. Neutron-diffraction study of triangular lattice systems $\text{Cu}(\text{Mn}_{1-x}\text{Cu}_x)\text{O}_2$, reveals a very rich spectrum of ground states as a function of temperature and chemical doping. It is confirmed that the stoichiometric phase CuMnO_2 undergoes a magnetoelastic transition from high-temperature monoclinic-paramagnetic to low temperature triclinic- antiferromagnetic phase. Upon substituting Cu for Mn, the structural distortion is gradually relaxed along with the antiferromagnetic coupling between adjacent MnO_2 layers. Upon increasing the doping level, the interlayer coupling changes from antiferromagnetic to ferromagnetic.

Noriki Terada, et.al.[38] (2011) have studied the magnetic correlations of the isosceles triangular lattice antiferromagnet $\text{Cu}_{1+x}\text{Mn}_{1-x}\text{O}_2$ with $x = 0.00$ and 0.04 , using the magnetic susceptibility, specific heat, elastic, and inelastic neutron-scattering experiments. In the neutron diffraction measurements on CuMnO_2 , the diffuse scattering observed in $T_N < T < 300$ K is well fitted by Warren function, proving the 2D short-range ordering. The magnetic correlations above T_N in both samples are characterized by 2D short-range order with strong spin fluctuations. In

the low-temperature region compared with T_N and the spin-wave gap, $C_{\text{mag}}(T)$ is proportional to T^2 . For two dimensionality and the linear dispersion relation, the $C_{\text{mag}}(T) \propto T^2$ can be explained, which is generally seen in spin-liquid-like systems and its conclude that the magnetic excitation below T_N is characterized by not only collective spin-wave excitation with 6 meV energy gap from the 3D long-range magnetic order, but also spin-liquid-like 2D excitation in CuMnO_2 .

F. Damay, et.al.[39] (2009) have reported neutron diffraction investigation versus temperature of the crystal and magnetic structures of CuMnO_2 . Around 80K, low-dimensionality magnetic scattering is observed, followed by three-dimensional magnetic ordering at $T_N=65$ K, characterized by the propagation vector $\mathbf{k}_1=(-1/2,1/2,1/2)$. Two-dimensional 2D square lattice can also be considered as equivalent to the anisotropic triangular lattice with two in-plane magnetic exchange interactions. In this configurations, J_1 along two of the triangle directions and J_2 along the third one $J_1 \neq J_2$, $(J_1, J_2) < 0$. Neutron powder diffraction investigation of CuMnO_2 has shown that at $T_N=65$ K, long range 3D magnetic ordering occurs simultaneously with a lowering of the monoclinic symmetry to a triclinic one. The corresponding lattice distortion, which affects the symmetry and distances of the Mn sublattice within the (a,b) plane, results in the differentiation of the antiferromagnetic and ferromagnetic bond lengths below T_N .

H. Hiraga, et.al.[40] (2009) have reported on the epitaxial growth and the optical and magnetic properties of CuMnO_2 thin films grown on MgAl_2O_4 substrates by a pulsed laser deposition method. The ultraviolet-visible optical response revealed a distinct absorption peak at 4.5 eV presumably with excitonic nature and broad peaks at 3.0 and 3.7 eV belongs to O $2p$ -Mn $3d$ charge transfer excitation. Small magnetic hysteresis with remanent magnetization of $0.04\mu\text{B}/\text{Mn}$ was observed below 20K, featuring canted antiferromagnetic spin ordering. Therefore, an epitaxial thin film of the layered compound involving magnetic and excitonic characteristics is available to explore the emerging functionality.

1.2 Theoretical Background:

1.2.1 Multiferroics

Electricity and magnetism were combined into one common entity in the 19th century, Maxwell combined electricity and magnetism into one common discipline through his well known equations (Maxwell's equations), meanwhile electric and magnetic ordering in solids are most oftenly considered separately, the electric charges of electrons and ions are responsible for the charge effects, whereas electron spins leads to magnetic properties. But there are cases where these two distinctly different degrees of freedom (charge and spin) control one another (as in the field of spintronics where the effect of spin controls transport property of the solid and vice-versa). The finding of strong coupling between magnetic and electric degrees of freedom in insulators can be traced back to Pierre Curie: but in real sense, it all started in 1959 with the short remark by Landau and Lifshitz [41]: According to their theory, there are two class of coupling viz, linear coupling between magnetic and electric fields while other coupling belongs to piezomagnetism which consists of linear coupling between a magnetic field in a solid and a deformation (analogous to piezoelectricity). Both these phenomena could exist for certain classes of magnetocrystalline symmetry. In 1960, Dzyaloshinskii predicted [42], while Astrov and Folen observed [43,44] this type of coupling (named linear magnetoelectric coupling) in antiferromagnetic Cr_2O_3 . This finding was followed by the discovery of compounds like DyPO_4 [45], FeSb_2O_4 [46] and many more [47-55] having this type of coupling. The idea, that not only cross-coupling of responses (i.e., the appearance of magnetization \mathbf{M} in an electric field \mathbf{E} , or appearance of electric polarization \mathbf{P} by the application of magnetic field \mathbf{H}) can exist in solids, but also the systems in which two types of ordering: (ferro)magnetism (spontaneous magnetization) and ferroelectricity (spontaneous polarization), can coexist simultaneously in one material in the absence of external electric and magnetic fields. Schmid [56] introduced a name multiferroics for these materials (Fig. 1.1). The interest in this field had been slowed down by 1970's, but mainly three events revived the interest in this field of multiferroics: One was that is, why the coexistence of magnetism and ferroelectricity is so rare in nature [57,58]. The other two were experimental discoveries those introduced two distinct

classes of multiferroics. Ramesh's group (in 2003) grew thin films of one of the most popular multiferroics, BiFeO_3 . Multiferroic properties of BiFeO_3 in the thin film form are much more enhanced as compared to the bulk BiFeO_3 whose multiferroic properties are very weak [59]. The discovery of a fascinating class of multiferroics, (2003) in which magnetism and ferroelectricity do not just coexist, but in which magnetism causes ferroelectricity. Tokura and Kimura discovered this phenomenon in TbMnO_3 and Cheong found a similar effect in TbMn_2O_5 .

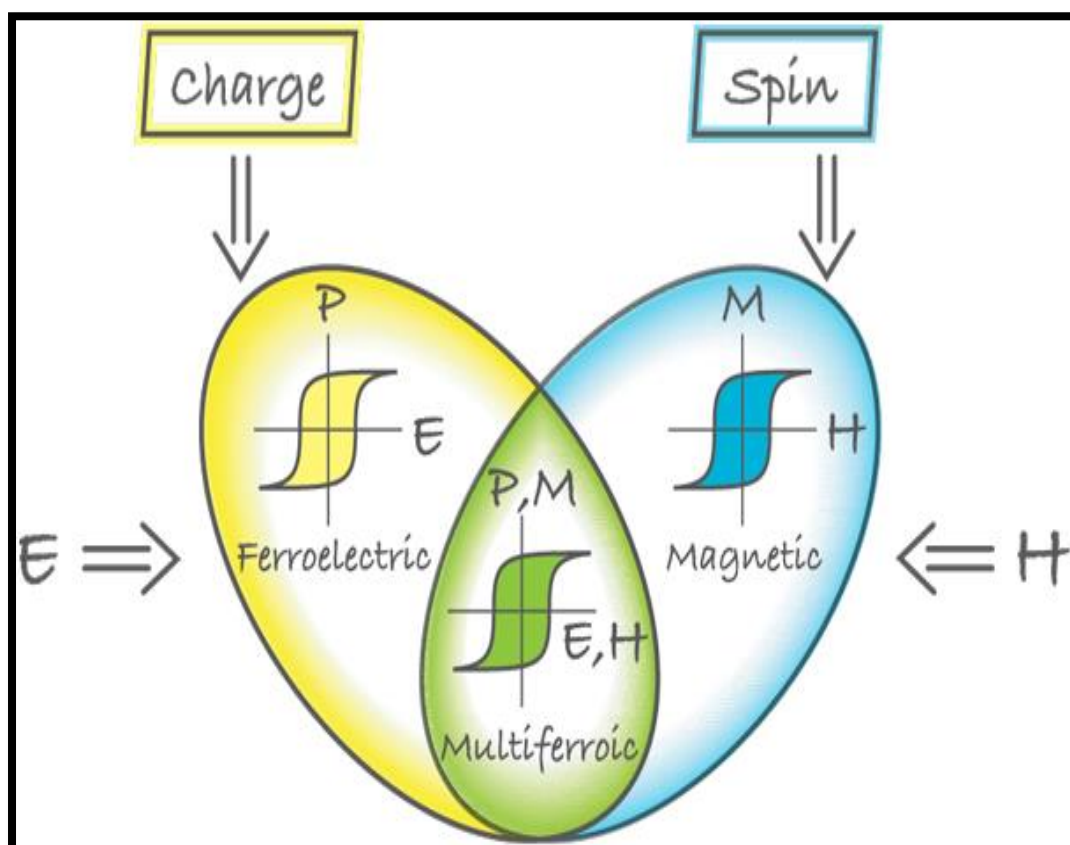


Fig.1.7. Schematic diagram of multiferroic materials which combine the properties of ferroelectrics and magnets (Courtesy: Khomskii, D., *Physics 2*, 20-27, 2009) [58].

Multiferroics combine the properties of ferroelectrics and magnets. In the ideal case, the magnetization of a ferromagnet in a magnetic field displays the usual hysteresis (blue), and ferroelectrics have a similar response to an electric field (yellow). If we manage to create multiferroics that are simultaneously ferromagnetic and ferroelectric (green), then there is a magnetic response to an electric field, or, electric response to an magnetic field which leads to the modification of polarization by magnetic field.

Using the above phenomena, creation of new 4-state logic state: (i.e., with both up and down polarization and up and down magnetization).

Multiferroic materials with cross-coupling effect (magnetoelectric coupling), have significant potential for practical applications which include the ability to address magnetic memory electrically, and magnetoelectric sensors. Magnetoelectric sensors are widely used in the field of biomedical instruments.

1.2.2 Symmetry Consideration

Each multiferroic property is closely connected to symmetry. The primary ferroic properties can be characterized by their behavior under space and time. Space inversion will reverse the direction of polarization \mathbf{p} while leaving the magnetization \mathbf{m} invariant. Time reversal, in turn, will change the sign of \mathbf{m} , while the sign of \mathbf{p} remains invariant.

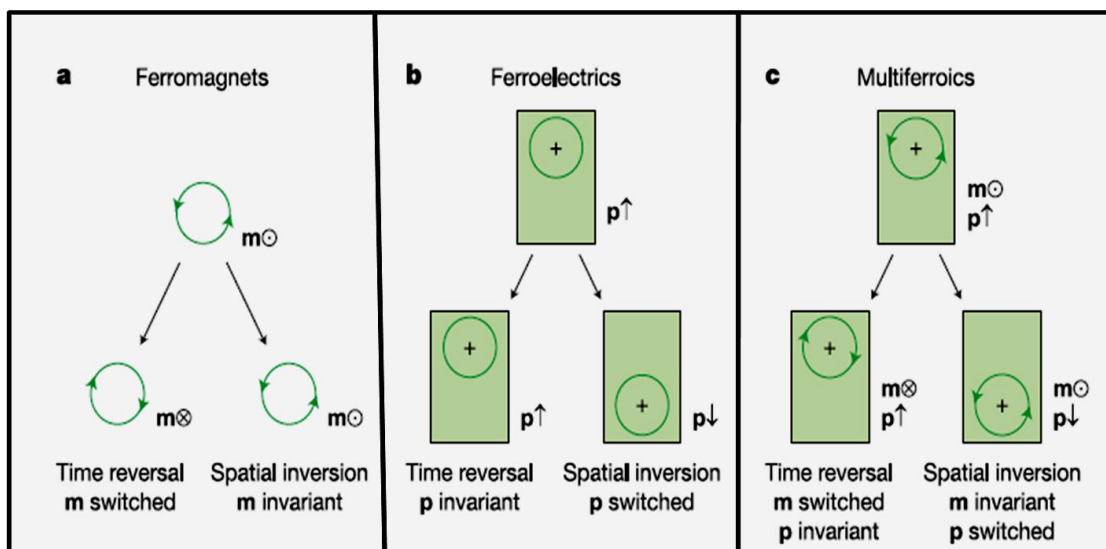


Fig.1.8. Time-reversal and spatial-inversion symmetry in ferroics (Courtesy: Eerenstein, W., Mathur, N. and Scott, J., *Nature* 442, 759-765, 2006) [60].

Ferromagnets: The local magnetic moment \mathbf{m} may be represented classically by a charge that dynamically traces an orbit, as indicated by the arrowheads [Fig 1.3(a)]. A spatial inversion produces no change, but time reversal switches the orbit and thus \mathbf{m} changes its sign.

Ferroelectrics: The local dipole moment \mathbf{p} may be represented by a positive point charge that lies asymmetrically within a crystallographic unit cell that has no net charge. There is no net time dependence, but spatial inversion reverses \mathbf{p} [Fig. 1.3(b)].

Multiferroics: Both ferromagnetic and ferroelectric possess neither symmetry [Fig. 1.3(c)] [31].

Magnetoelectric multiferroics require simultaneous violation of space and time inversion symmetry. To understand the basic phenomena in the field of multiferroics, it is necessary to classify multiferroics by the microscopic mechanism that determines their properties.

1.2.3 Types of Multiferroics:

The microscopic origin of magnetism is basically the same in all magnets: it is the presence of localized electrons, mostly in the partially filled d or f shells of transition-metal ions or rare-earth ions, which have a corresponding localized spin, or magnetic moment. Exchange interactions between the localized moments lead to magnetic order. The situation in ferroelectrics is quite different. There are several different microscopic sources of ferroelectricity, and accordingly one can have different types of multiferroics. In general, there are two groups of multiferroics, the first group, called type-I multiferroics, contains those materials in which ferroelectricity and magnetism have different sources and appear significantly independent of one another, although there is some coupling between them. The first one corresponds to the compounds with spontaneous polarization (T_C ferroelectric) appearing above the magnetic ordering temperature (T_C or T_N ferro(antiferro)magnetic), such as BiFeO_3 ($T_{FE} \sim 1100\text{K}$, $T_N = 643\text{K}$, $P \sim 90\ \mu\text{C}/\text{cm}^2$) and YMnO_3 ($T_{FE} \sim 914\text{K}$, $T_N = 76\text{K}$, $P \sim 6\ \mu\text{C}/\text{cm}^2$). The second group or type-II multiferroics, is relatively recently discovered materials, in which magnetism causes ferroelectricity, implying a strong coupling between the two. However, the polarization in these materials is usually much smaller ($10\text{-}2\ \mu\text{C}/\text{cm}^2$). Different types of compounds, in type-II multiferroics ranging from vanadates to cuprates: spinel vanadates CdV_2O_4 [61], FeV_2O_4 [62], chromites with the spinels ACr_2O_4 ($A = \text{Cu}, \text{Fe}, \text{Ni}$) [63-66] and the $\text{A}'\text{CrO}_2$ delafossites ($A' = \text{Li}, \text{Cu}, \text{Ag}$) [67], Ortho manganites RMnO_3 with ($R = \text{Tb}$

and Dy)[68,69], RMn_2O_5 with (R = Tb, Gd, ...)[70-73], $\text{CaMn}_7\text{O}_{12}$ quadruple perovskite[74], MnWO_4 [75], Ferrites with GaFeO_3 [76], Orthoferrites such as GdFeO_3 [77], CuFeO_2 [78] and the corresponding doped delafossites of $\text{CuFe}_{1-x}\text{MxO}_2$ formula (M = Al, Ga, Rh)[79-81], ordered perovskites RBaCuFeO_5 [82-83], the mixed manganite cobaltite $\text{Ca}_3\text{CoMnO}_6$ [84], a chain compound with Co/Mn ordering in the magnetic chains, the cobaltites $\text{Ba}_2\text{CoGe}_2\text{O}_7$ [85], $\text{Ca}_2\text{CoSi}_2\text{O}_7$ [86], LiCoPO_4 [87], $\text{CaBaCo}_4\text{O}_7$ [88] the nickelate $\text{Ni}_3\text{V}_2\text{O}_8$ [89], Cuprates with the CuO tenorite [90] and LiCuVO_4 [91].

1.2.3.1 Type-I Multiferroics:- There are several subclasses of type-I multiferroics, depending on the mechanism of ferroelectricity in them.

(1) Multiferroic Perovskites (d^0 vs d^n)

(2) Ferroelectricity Due to Lone Pairs

(3) Ferroelectricity Due to Charge Ordering

(4) Geometric Ferroelectricity

Multiferroic Perovskites (d^0 vs d^n):

The microscopic origin of magnetism one needs partially filled d shells of a transition metal, all ferroelectric perovskites contain transition metal ions with an empty d shell, such as Ti^{4+} , Ta^{5+} , W^{6+} Ferroelectricity in these systems is caused by the off-center shifts of the transition metal ion, which forms strong covalent bonds with one (or three) oxygens, using their empty d states. Presence of real d electrons in d^n configurations of magnetic transition metals suppresses this process, preventing ferroelectricity in magnetic perovskites, generally called as “ d^0 vs d^n problem.” In mixed perovskites with ferroelectrically active d^0 ions (green circles) and magnetic d^n ions (red), shifts of d^0 ions from the centers of O6 octahedra (yellow plaquettes) lead to polarization (green arrows), coexisting with magnetic order (red arrows).

Ferroelectricity Due to Lone Pairs:

In materials like BiFeO_3 and PbVO_3 , the ordering of lone pairs (yellow lobes), of Bi^{3+} and Pb^{2+} ions (orange) leads to the polarization (green arrow). In BiFeO_3 , and probably in BiMnO_3 and PbVO_3 , Bi^{3+} and Pb^{2+} play the key role in the origin of ferroelectricity. In these ions, there are two outer 6s electrons that do not participate in chemical bonds which are called lone pairs or dangling bonds.

Ferroelectricity Due to Charge Ordering:

One more mechanism that can lead to ferroelectricity exhibiting charge ordering. When charges order in a non-symmetric fashion, they induce electric polarization. In charge ordered systems, the coexistence of inequivalent sites with different charges, and inequivalent (long and short) bonds, leads to ferroelectricity.

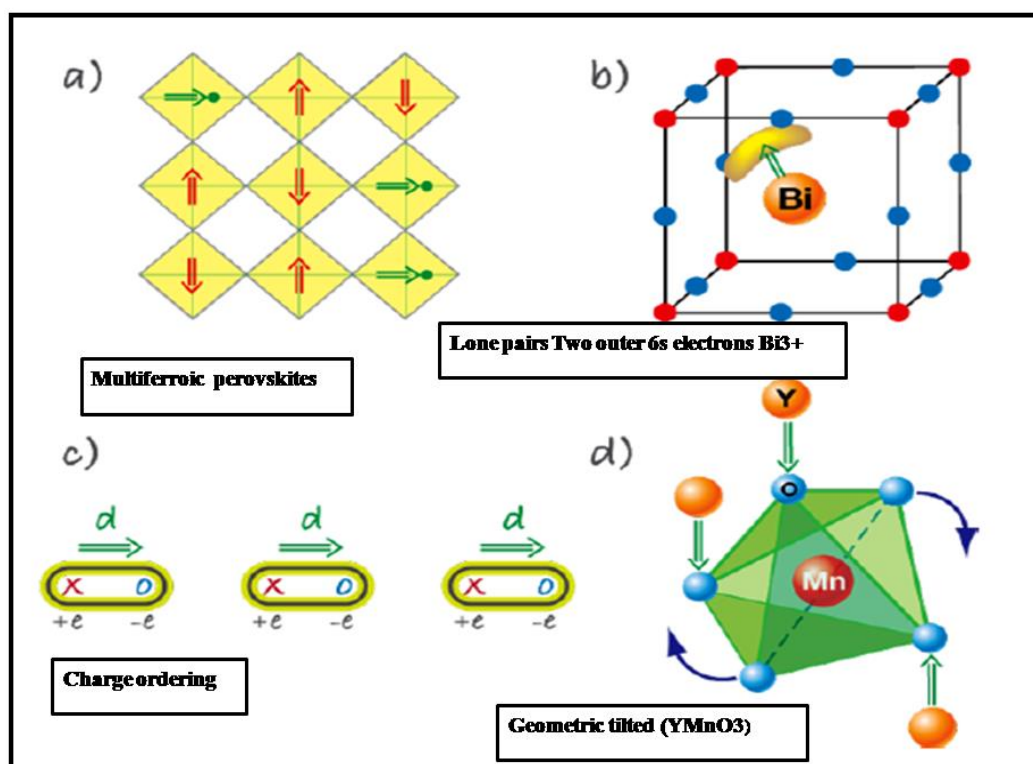


Fig.1.9. Depending upon the mechanism of origin of the ferroelectricity, type-I multiferroics have been divided in (a) Multiferroic perovskites (b) Ferroelectricity due to lone pairs (c) Ferroelectricity due to charge ordering and (d) Geometrically frustrated Ferroelectricity (Courtesy: Khomskii, D., Physics 2, 20-27, 2009) [58].

Geometric Ferroelectricity:

The geometric mechanism of generation of polarization in YMnO_3 describes the tilting of a rigid MnO_5 block with a magnetic Mn remaining at the center. Because of the tilting, the Y-O bonds form dipoles (green arrows), and there appears two down dipoles per one up dipole so that the system becomes ferroelectric (and multiferroic when Mn spins order at lower temperatures). Ferroelectricity in YMnO_3 has nothing to do with the magnetic Mn^{3+} but is caused by the tilting of the practically rigid MnO_5 block. This tilting occurs just to provide closer packing, and as a result, the oxygen ions move closer to the rather small Y ions.

1.2.4 Type-II Multiferroics: Magnetically Driven Multiferroics

There are two types of magnetically driven multiferroics are known possibility that an internal magnetic: (1) **Spiral Type-II Multiferroics** (2) **Collinear spin ordering**

1.2.4 .1 Spiral Type-II Multiferroics:

Microscopic mechanism of origin of ferroelectricity in these systems is not well known. It is well known fact that exhibit ferroelectricity in magnetic phases with spiral or helicoidal magnetic structure. In TbMnO_3 , there is no electric polarization with sinusoidal magnetic structure phase between 40 to 30 K but a finite polarization appears below 30K when magnetic structure changes from sinusoidal to helicoidal. Katsura, Nagaosa, and Balatsky, using a microscopic approach, and Mostovoy, using a phenomenological approach, showed that in a cycloidal spiral a polarization, \mathbf{P} , appears, that is given by:

$$\mathbf{P} \sim \mathbf{r}_{ij} \times (\mathbf{S}_i \times \mathbf{S}_j) \sim [\mathbf{Q} \times \mathbf{e}]$$

where \mathbf{r}_{ij} is the vector connecting neighboring spins \mathbf{S}_i and \mathbf{S}_j , \mathbf{Q} is the wave vector describing the spiral, and $\mathbf{e} \sim [\mathbf{S}_i \times \mathbf{S}_j]$ is the spin rotation axis.

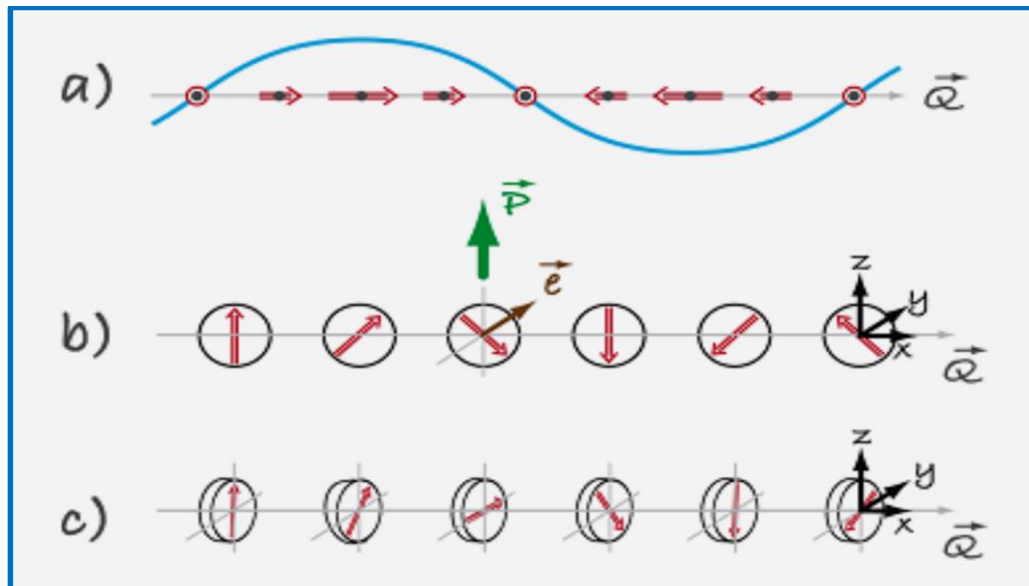


Fig.1.10. Different types of spin structures relevant for type-II multiferroics. (a) Sinusoidal spin wave, in which spins point along one direction but vary in magnitude. This structure is centrosymmetric and consequently not ferroelectric. (b) The cycloidal spiral with the wave vector $Q = Qx$ and spins rotating in the (x,z) -plane. It is in this case where one finds nonzero polarization, $P_z \neq 0$. (c) In a so-called proper screw the spins rotate in a plane perpendicular to Q . Here the inversion symmetry is broken, but most often it does not produce polarization, although in certain cases it might [53]. (Courtesy: Khomskii, D., Physics 2, 20-27, 2009) [58].

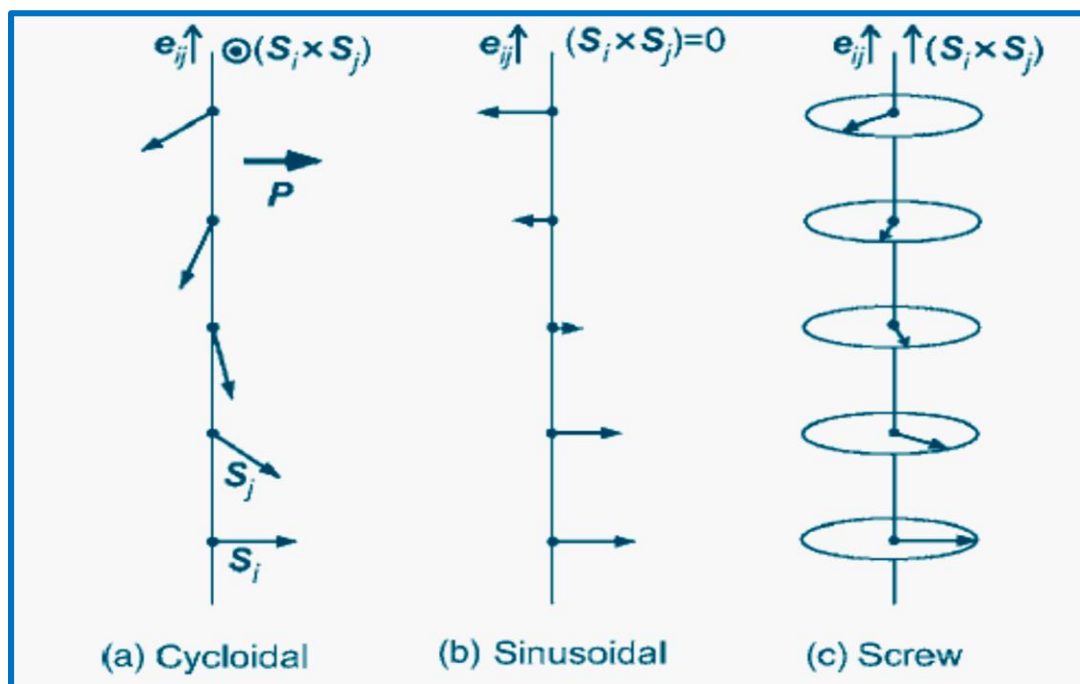


Fig.1.11. Geometric configurations of (a) Cycloidal (b) Sinusoidal (c) Screw type of magnetic structure. (Courtesy: Arkenbout A.H., Phys RevB, 74, 184431, 2006) [92]

The general relation between electric polarization P and magnetization M in systems with spiral magnetic structures has been deduced from

$$\vec{P} \propto \gamma \vec{e}_{ij} \times (\mathbf{S}_i \times \mathbf{S}_j).$$

here γ is a constant proportional to the spin orbit coupling and superexchange interactions, \vec{e}_{ij} is the unit vector connecting the neighbouring i and j sites, and \mathbf{S} is the magnetic moment. In this equation, \vec{e}_{ij} is along the propagation vector of the spiral structure, and $(\mathbf{S}_i \times \mathbf{S}_j)$ is parallel to the spin rotation axes. This indicates that a finite electric polarization can appear when the magnetic moments at sites i and j are coupled noncollinearly in a spiral manner, and the spin rotation axis is not parallel to the propagation vector. In case of cycloidal spiral magnetic structure, as shown in the fig.1(a), the direction of electric polarization is perpendicular to the spin rotation axis and the propagation vector of spiral, can be reversed by the change in the chirality of the spiral. In the case of collinear sinusoidal structure as shown in fig (b) in which $(\mathbf{S}_i \times \mathbf{S}_j)$ vanishes. Moreover in screw spiral structure \vec{e}_{ij} parallel to $(\mathbf{S}_i \times \mathbf{S}_j)$ which results \vec{P} vanishes as shown in fig(c). A detailed description of different class of magnetic structures as given in following figures:

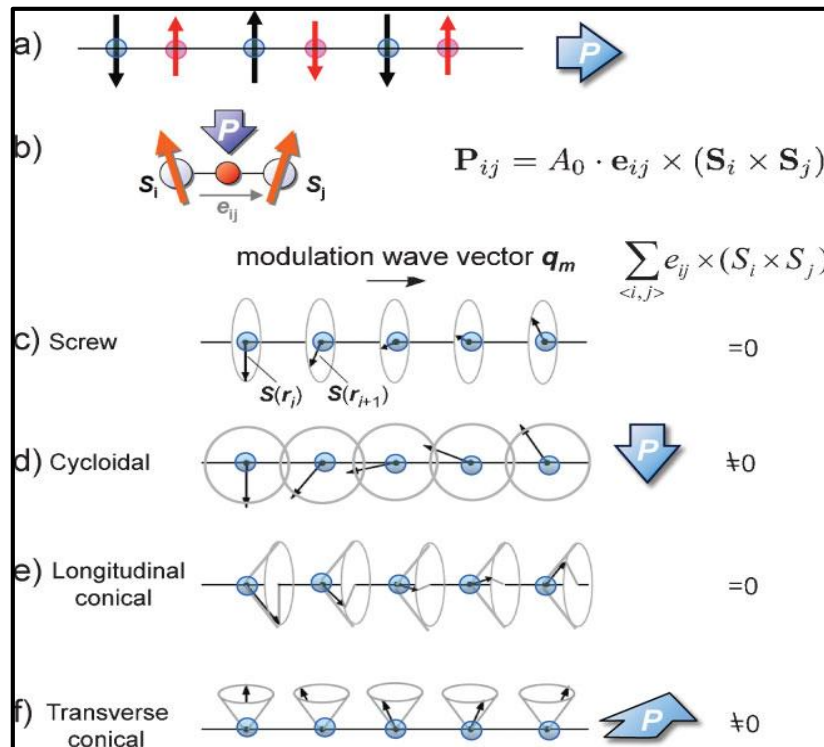


Fig.1.12. Schematic illustrations of types of spiral magnetic structures on a 1D array of magnetic moments $S(r)$. Inversion symmetry breaking by (a) collinear (b) noncollinear magnetic order and possible polarization direction. (d) proper-screw, (e) cycloidal, (f) longitudinal-conical, and (g) transverse-conical magnetic structure. The magnitudes of macroscopic polarization obtained from the spincurrent model or inverse DM model. (Courtesy: Tokura.Y.et.al; Adv.mater.22, 1554-65, 2010)[93]

1.2.4.2 Collinear spin ordering:

A strongly frustrated Ising spin chain with nearest-neighbour ferromagnetic and next-nearest neighbour antiferromagnetic coupling has the up-up-down-down ($\uparrow\uparrow\downarrow\downarrow$) ground state see Fig(a)

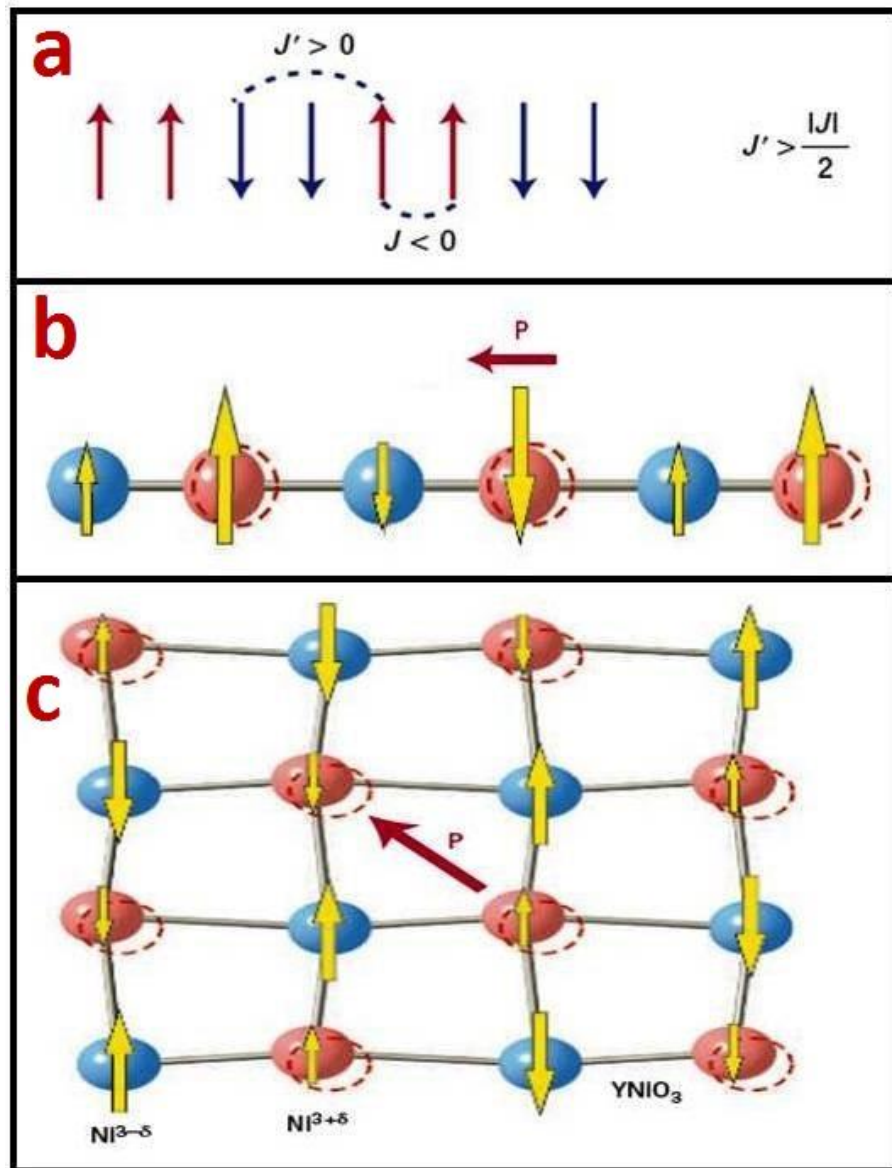


Fig.1.13. (a) Ising spin chain with nearest-neighbour ferromagnetic and next-nearest neighbour antiferromagnetic coupling has the up-up-down-down ($\uparrow\uparrow\downarrow\downarrow$) ground state (b) Ferroelectricity in charge ordered systems (c) Polarization induced by charge ordering and the ($\uparrow\uparrow\downarrow\downarrow$) type spin ordering in perovskite YNiO_3 (Courtesy: S.W.Cheong et al Nature materials 6, 2007)[94]

If the charges of magnetic ions or tilts of oxygen octahedra alternate along the chain, this magnetic ordering breaks inversion symmetry on magnetic sites and induces electric polarization (Fig. b). For magnetic spirals, ions are displaced by exchange striction, which shortens bonds between parallel spins and stretches those connecting antiparallel spins in the $\uparrow\uparrow\downarrow\downarrow$ state. In the Landau description, the coupling term inducing the polarization has the form of $P(L_1^2 - L_2^2)$, typical for improper ferroelectrics where $\mathbf{L}_1 = \mathbf{S}_1 + \mathbf{S}_2 - \mathbf{S}_3 - \mathbf{S}_4$ and $\mathbf{L}_2 = \mathbf{S}_1 - \mathbf{S}_2 - \mathbf{S}_3 + \mathbf{S}_4$ represent two possible configurations of the $\uparrow\uparrow\downarrow$ or $\downarrow\downarrow\uparrow$ order. It would be worthwhile to explore multiferroics in which ferroelectricity appears as a combined effect of charge and magnetic ordering that together break inversion symmetry. It is obvious that, site-centred charge ordering coexisting with the spin ordering of the up–up–down–down type has been observed in perovskites RNiO_3 .

1.2.5 Antisymmetric Dzyaloshinskii–Moriya (DM) interaction:

In the antisymmetric Dzyaloshinskii–Moriya (DM) interaction, $\mathbf{D}_{n,n+1} \cdot \mathbf{S}_n \times \mathbf{S}_{n+1}$, where $\mathbf{D}_{n,n+1}$ is the Dzyaloshinskii vector (50,51). This interaction is a relativistic correction to the usual super exchange and its strength is proportional to the spin–orbit coupling constant. The DM interaction favours non-collinear spin ordering. The Dzyaloshinskii vector $\mathbf{D}_{n,n+1}$ is proportional to $\mathbf{x} \times \mathbf{r}_{n,n+1}$, where $\mathbf{r}_{n,n+1}$ is a unit vector along the line connecting the magnetic ions n and $n+1$, and \mathbf{x} is the shift of the oxygen ion from this line (Fig.1.15). Thus, the energy of the DM interaction increases with \mathbf{x} , describing the degree of inversion symmetry breaking at the oxygen site. Because in the spiral state the vector product $\mathbf{S}_n \times \mathbf{S}_{n+1}$ has the same sign for all pairs of neighbouring spins, the DM interaction pushes negative oxygen ions in one direction perpendicular to the spin chain formed by positive magnetic ions, thus inducing electric polarization perpendicular to the chain. This mechanism can also be expressed in terms of the spin current, $\mathbf{j}_{n,n+1} \propto \mathbf{S}_n \times \mathbf{S}_{n+1}$, describing the precession of the spin \mathbf{S}_n in the exchange field created by the spin \mathbf{S}_{n+1} . The induced electric dipole is then expressed as $\mathbf{P}_{n,n+1} \propto \mathbf{r}_{n,n+1} \times \mathbf{j}_{n,n+1}$ (ref. 24).

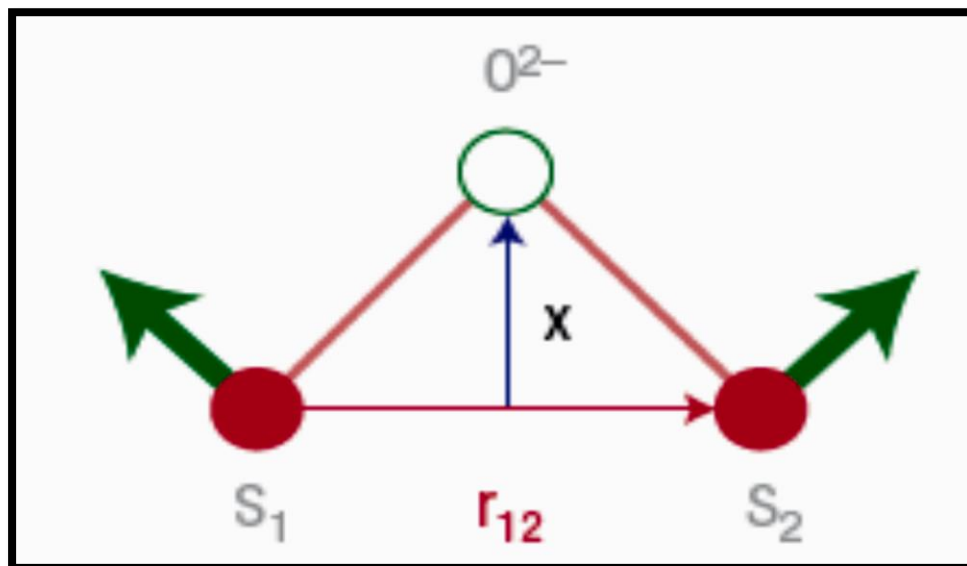


Fig:1.15. Effects of the antisymmetric Dzyaloshinskii–Moriya interaction. (Courtesy: S.W.Cheong *et.al*, *Nature materials* 6, 2007)[94]

Three possible mechanisms have been proposed for the coupling between magnetic and electric moments for the ME multiferroic materials:

- (1) **Magnetostriction model**
- (2) **spin-current model**
- (3) **Spin-dependent d-p hybridization**

(1) Magnetostriction model:

In this model, ferroelectricity is induced in collinear-commensurate magnetic structures. Electric dipole moment is given by

$$C(r)(\mathbf{S}_i \cdot \mathbf{S}_{i+1}),$$

where $C(r)$ is a constant dependent on the local crystal structure and the exchange interactions. The spontaneous electric polarization observed in the collinear-commensurate magnetic orderings in orthorhombic HoMnO_3 .

(2) Spin-current model:

In this model, ferroelectricity is induced between two non-collinearly aligned neighboring spins \mathbf{S}_i and \mathbf{S}_{i+1} generate a local electric dipole moment \mathbf{p} given by

$$\mathbf{P} \propto \mathbf{e}_{i,i+1} \times (\mathbf{S}_i \times \mathbf{S}_{i+1})$$

where $\mathbf{e}_{i,i+1}$ is the unit vector connecting the two spins. This formula predicts macroscopic uniform electric polarization in a magnetic structure with cycloidal spin components, and shows excellent agreement with the experimentally determined

relationships between magnetic structures and electric polarization in various transition metal oxides, such as TbMnO_3 , $\text{Tb}_{1-x}\text{Dy}_x\text{MnO}_3$, $\text{Ni}_3\text{V}_2\text{O}_8$, MnWO_4 , and CoCr_2O_4 .

(3) Spin-dependent d-p hybridization:

It is proposed that the electric polarization might be induced through the variation of the metal-ligand hybridization,

$$\mathbf{P} \sim (\mathbf{S}_i \cdot \mathbf{e}_{ij})\mathbf{S}_i - (\mathbf{S}_j \cdot \mathbf{e}_{ij})\mathbf{S}_j$$

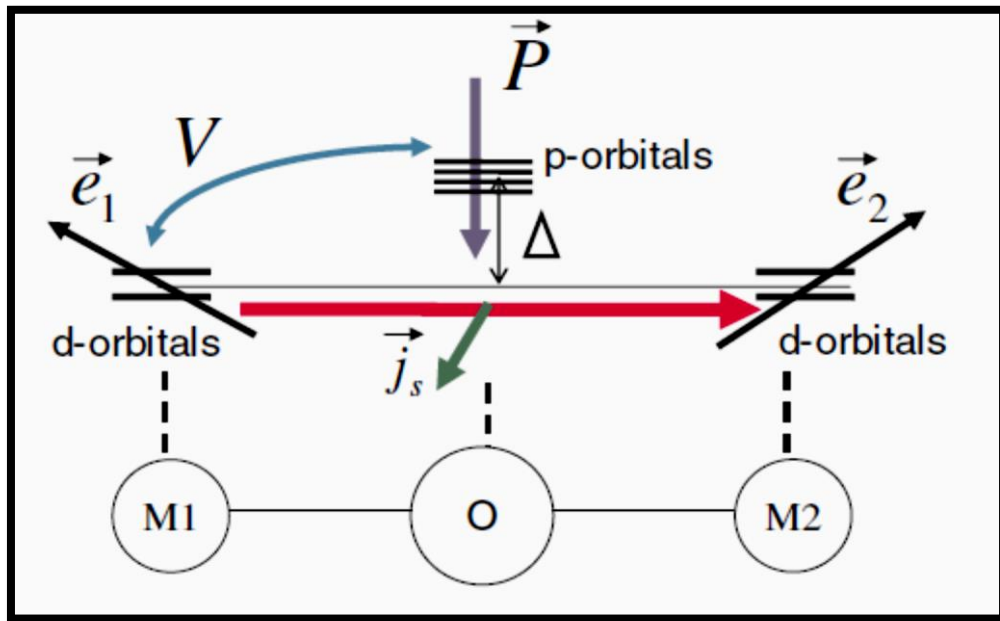


Fig.1.16. The cluster model with two transition metal ions M_1 and M_2 with oxygen atom between them. Electric dipole induction through hybridization of p-d orbital (Courtesy: Hosho Katsura et.al, *PhysRevLett*, 95, 57205, 2005)[95]

The cluster model having two transition metal ions M_1 , M_2 with the oxygen atom O between them. With the noncollinear spin directions \vec{e}_1 and \vec{e}_2 , there arises the spin current $\vec{J}_s \propto \vec{e}_1 \times \vec{e}_2$ between M_1 and M_2 . Here the direction of the vector \vec{J}_s is that of the spin polarization carried by the spin current. The direction of the electric polarization \vec{P} is given by $\vec{P} \propto \vec{e}_{12} \times \vec{J}_s$ where \vec{e}_{12} the unit vector is connecting M_1 and M_2 .

1.2.6 Magnetoelectric coupling:

Magnetoelectric (ME) effect is obtained from the expansion of the free energy of a material, ie

$$\begin{aligned} \vec{F}(\vec{E}, \vec{H}) &= F_0 - P_i^S E_i - M_i^S H_i - \frac{1}{2} \mu_0 \mu_{ij} H_i H_j - \frac{1}{2} \epsilon_0 \epsilon_{ij} E_i E_j - \alpha_{ij} E_i H_j - \alpha_{ij} E_i H_j \\ &\quad - \frac{1}{2} \beta_{ijk} E_i H_j H_k - \frac{1}{2} \gamma_{ijk} H_i E_j E_k - \dots \dots \\ P_i(\vec{E}, \vec{H}) &= - \left(\frac{\partial F}{\partial E_i} \right) \\ &= P_i^S + \epsilon_0 \epsilon_{ij} E_j + \alpha_{ij} H_j + \frac{1}{2} \beta_{ijk} H_j H_k + \gamma_{ijk} H_i E_j - \dots \dots \\ M_i(\vec{E}, \vec{H}) &= - \left(\frac{\partial F}{\partial H_i} \right) \\ &= M_i^S + \mu_0 \mu_{ij} H_j + \alpha_{ij} E_j + \beta_{ijk} E_i H_j + \frac{1}{2} \gamma_{ijk} E_j E_k - \dots \dots \end{aligned}$$

where P_i^S and M_i^S represent the spontaneous polarization, where as ϵ_{ij} and μ_{ij} are the electric and magnetic susceptibilities. Differentiation with respect to the fields leads to electric and magnetic polarization. The tensor α_{ij} denote the induction of polarization by a magnetic field or of magnetization by an electric field is known as linear ME effect. In case of antiferromagnetic, value of spontaneous polarizations P_i^S and M_i^S vanishes. Which shows that in zero electric field, a magnetic field can induce a finite polarization, $P_i = \alpha_{ij} H_j$ and vice versa, in zero magnetic field an electric field can induce a finite magnetization, $M_i = \alpha_{ij} E_j$. Permittivity of free space is denoted ϵ_0 , and the relative permittivity ϵ_{ij} is a second-rank tensor that is typically independent of E_i in non-ferroic materials. The second term is the magnetic equivalent of the first term, where μ_{ij} is the relative permeability and μ_0 is the permeability of free space. The third term describes linear magnetoelectric coupling via α_{ij} , the third-rank tensors β_{ijk} and γ_{ijk} represent higher-order (quadratic) magnetoelectric coefficients. For **non-ferroic material**, where both the temperature-dependent electrical polarization $P_i(T) \frac{\mu C}{m^2}$ and the magnetization $M_i(T)$ (μ_B per formula unit, where μ_B is the Bohr magneton) are zero in the absence of applied fields and there is no hysteresis.

$$\vec{F}(\vec{E}, \vec{H}) = -\frac{1}{2}\mu_0\mu_{ij}H_iH_j - \frac{1}{2}\alpha_{ij}E_iE_j - \alpha_{ij}E_iH_j - \frac{1}{2}\beta_{ijk}E_iH_jH_k - \frac{1}{2}\gamma_{ijk}H_iE_jE_k - \dots$$

magnetolectric coefficients incorporate the field independent material response functions ϵ_{ij} and μ_{ij} . The magnetolectric effects can then easily be established in the form $P_i(H_j)$ or $M_i(E_j)$. One obtains:

$$P_i = \alpha_{ij}H_j + \frac{\beta_{ijk}}{2}H_jH_k + \dots$$

and

$$\mu_0 M_i = \alpha_{ji} + \frac{\gamma_{ijk}}{2}E_jE_k + \dots$$

In ferroic materials, ϵ_{ij} and μ_{ij} display field hysteresis. Moreover, ferroics are better parameterized in terms of resultant rather than applied fields. This is due to the fact that, it is possible to account for the potentially significant depolarizing/demagnetizing factors in infinite media, and also because of coupling constants would be functions of temperature alone, as in standard Landau theory. A **multiferroic** that is ferromagnetic and ferroelectric is liable to display large linear magnetolectric effects. This follows because ferroelectric and ferromagnetic materials often (but not always) possess a large permittivity and permeability respectively and α_{ij} is bounded by the geometric mean of the diagonalized tensors ϵ_{ij} and μ_{ij} such that:

$$\alpha^2 \leq \epsilon_0\mu_0\epsilon_{ii}\mu_{jj}$$

Equation (4) is obtained from equation (1) by forcing the sum of the first three terms to be greater than zero, i.e., ignoring higher-order coupling terms.

1.2.7 Magnetism:

The Delafossites (ABO₂-type materials) and distorted delafossites or Crednerite structure materials such as CuFeO₂, CuCrO₂ and CuMnO₂ have a magnetic ordering from paramagnetic to antiferromagnetic. Different materials show different response when they are exposed under magnetic field. In atom, the orbital motion of the electron, the change of the orbital due to the magnetic field and the spin of the electron will affect the magnetic moment of the atom. When all electrons in the atom

are paired then the magnetic spins will cancel each other leads to total magnetic moments will be zero. Moreover an unpaired electron which is not fetches into atom have a magnetic moment.

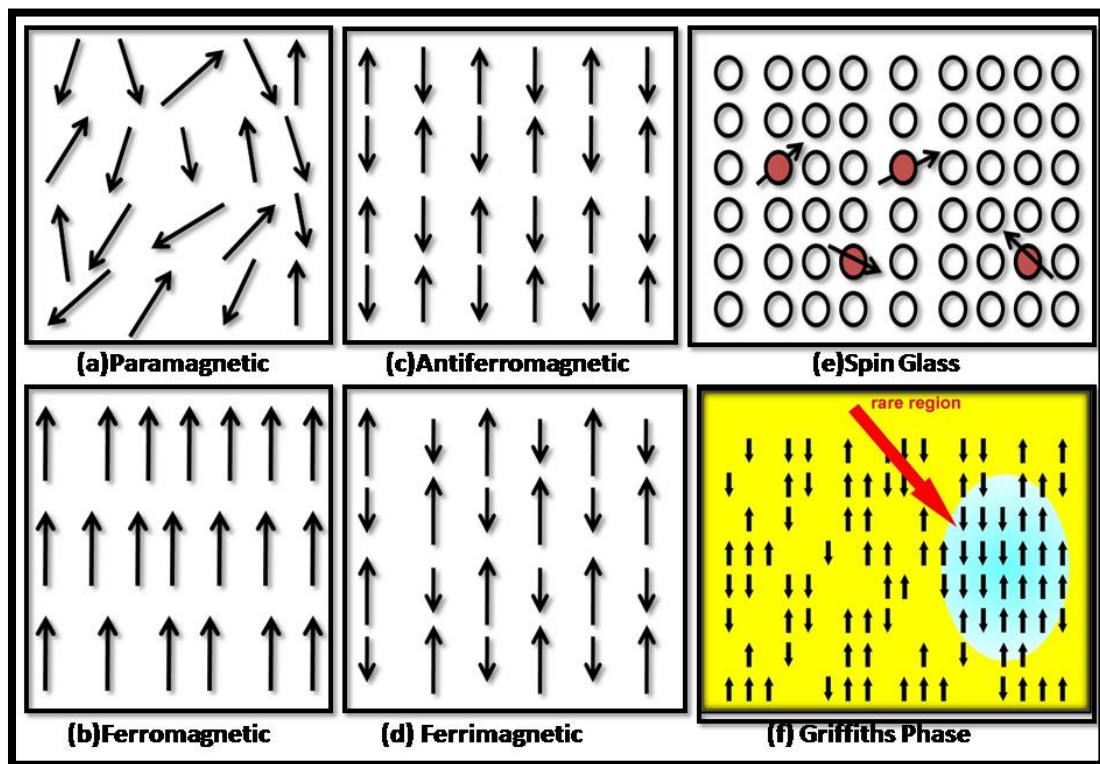


Fig.1.17. Schematic diagram of various spin configuration (a) Paramagnetic (b) Ferromagnetic (c) Antiferromagnetic (d) Ferrimagnetic (e) Spin Glass and (f) Griffith phase.

In general, different ground states coexist include such as, paramagnetic, ferromagnetic, antiferromagnetic, ferrimagnetic, spin glass, griffith phase, spiral and helical structures. In diamagnetic material, all the electrons are paired or the orbital shells are filled so there is no net magnetic moment. Diamagnetic material has weak, negative magnetic susceptibility and it will be repelled in the magnetic field. In paramagnetic material, some of the atoms or ions have unpaired electrons and the orbital shells are partially filled. Paramagnetic material has small, positive magnetic susceptibility and it is slightly attracted in the magnetic field. Ferromagnetic material has strong, positive magnetic susceptibility and strongly attracted in magnetic field. In addition, ferromagnetic material will retain its magnetic properties after the magnetic field is removed. In the normal condition, without magnetic field, the magnetic

domains in the ferromagnetic material are organized randomly. However, when we put a ferromagnetic material in the magnetic field, all the magnetic domains in the ferromagnetic material will eventually be parallel in the same direction. Further, when we remove the magnetic field, some domains are still pointing in the same direction. Spiral and helical structures in which the direction of the magnetic moment precesses around a cone or a circle as one moves from one site to the next. In spin glasses, magnetic moments lie in frozen random arrangements at a well defined temperature known as freezing temperature below which a metastable frozen state appears without the usual magnetic long range ordering. In an antiferromagnetic material, in which the magnetic moments are equal and antiparallel alignment, creating a zero net magnetic moment.

1.2.7.1 Landau theory of ferromagnetism (Mean Field Theory):

$$F(M) = F_0 + a(T)M^2 + bM^4$$

where F_0 and b are constants ($b > 0$) and $a(T)$ is temperature dependent parameter. It can be shown that system yields proper transition if $a(T)$ can be expressed as $a(T) = a_0(T - T_c)$ where a_0 is a positive constant.

It is necessary to minimize the free energy,

$$\frac{\partial F}{\partial M} = 0$$

$$2M[a_0(T - T_c) + 2bM^2] = 0$$

$$M = 0 \text{ or } M = \pm \left[\frac{a_0(T_c - T)}{2b} \right]^{1/2}$$

The second is only valid when $T < T_c$. The first condition applies above or below T_c but below T_c it only produces a position of unstable equilibrium ($\frac{\partial^2 F}{\partial^2 M}$). For $T > T_c$, Thus the magnetization follows the curve it is zero and is non-zero and proportional to $(T_c - T)^{1/2}$ for $T < T_c$.

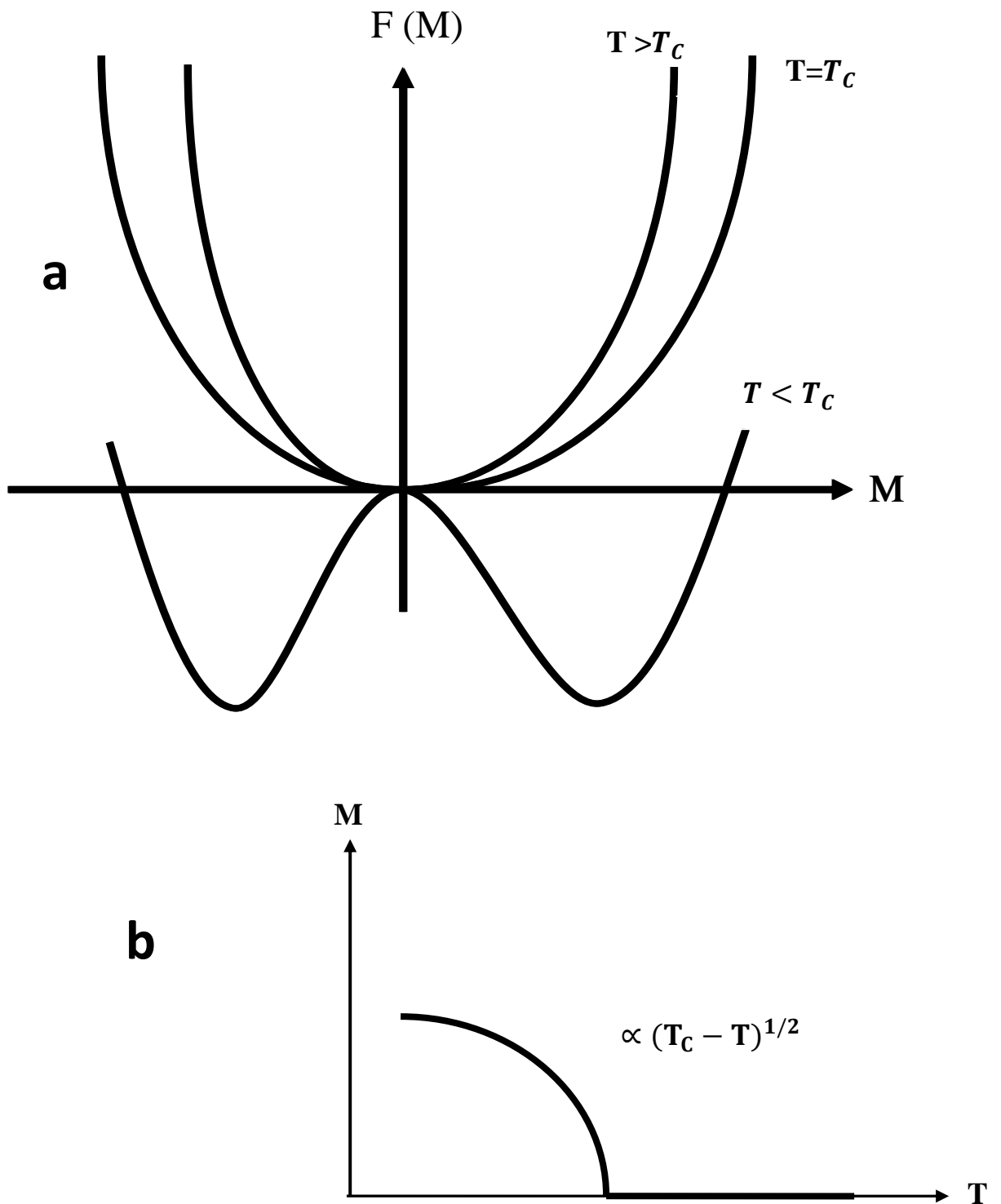


Fig.1.18. (a) Free energy $F(M)$ of a ferromagnet (b) Magnetization as a function of temperature[96]

1.2.7.2 Heisenberg model:

In order to estimate the exchange interaction parameters within the Mn triangular layers and the interlayer exchangesuch as in case of CuMnO₂.The total energies of different magnetic configurations are estimated using Heisenberg model has expressed as

$$\hat{H} = - \sum_{\langle ij \rangle} J_{ij} \mathbf{S}_i \cdot \mathbf{S}_j$$

The in-plane exchange constants J_1 and J_2 were recalculated from the total energies of three different configurations of magnetic structures: (1) fully ferromagnetic, (2) Mn ions along the short (long) Mn–Mn bond have ordered ferromagnetically (antiferromagnetically), and (3)Mn ions along the short Mn–Mn bonds have antiferromagnetically coupled.

1.2.7.3 Ising Models:

In this model the spins are only allowed to point up or down, i.e. only z component of the spin is being considered. The Hamiltonian of this model is

$$H = - \sum_{\langle ij \rangle} J S_i^z S_j^z$$

The operator for the z component of the spin was written as S_z . If the Ising spins are placed on a one-dimensional lattice, there is no phase transition. First, consider a chain with $N + 1$ spins .The Hamiltonian is

$$H = -2J \sum_{i=1}^N S_i^z S_{i+1}^z$$

1.2.7.4 Landau theory of phase transitions: This theory deals with behavior of the ferromagnetic.This is a mean-field theory in which an identical exchange field is felt by all spins. This leads to the magnetization behaving as $(T_c - T)^{1/2}$ below the transition.In real systems it is found that the magnetization does behave as $(T_c - T)^\beta$ close to the transition, but the exponent β is not necessarily equal to $1/2$.The exponent therefore gives important information about the nature of the phase transition. A number of other similar exponents, known as critical exponents, can be defined. Thus near the phase transition temperature T_c it is found experimentally that

$$\chi \propto (T - T_c)^{-\gamma}, \quad T > T_c$$

$$M \propto (T_c - T)^\beta, \quad T < T_c$$

$$M \propto H^{1/\delta}, \quad T = T_c$$

where β, γ and δ are the critical exponents.

Critical exponents of various models:

Model	Mean field	Ising	Heisenberg
D	any	1	3
d	any	2	3
β	1/2	1/8	0.367
γ	1	7/4	1.388(3)
δ	3	1.5	4.78

1.2.8 Exchange bias phenomenology:

The exchange bias (EB) effect, also known as unidirectional anisotropy, was discovered in 1956 by Meiklejohn and Bean [97-99]. They proposed a model to account for the magnitude of the hysteresis shift of the FM/AFM systems. It was observed that Co particles embedded in their native antiferromagnetic oxide CoO fetches the hysteresis shift into the system. The EB effect was observed in a variety of systems containing ferromagnetic (FM)/antiferromagnetic (AFM) interfaces, such as small particles [100], inhomogeneous materials, FM thin films on AFM single crystals and thin films. In addition to FM/AFM interfaces, exchange bias and related effects have also been observed in other types of interfaces, e.g. involving ferrimagnets (ferri): ferri/AFM, FM/ferri or diluted magnetic semiconductors (DMS): DMS/AFM.

Phenomenological model of EB:-

Interface coupling due to exchange anisotropy is observed cooling the AFM-FM couple in the presence of a static magnetic field from a temperature above T_N , but below T_c ($T_N < T < T_c$) to temperature $T < T_N$. The hysteresis loop of the AFM-FM system at $T < T_N$ is shifted along the field axis in the opposite direction to the cooling field. This loop shift is generally known as exchange bias H_E . When a field is applied in the temperature range $T_N < T < T_c$, the FM spins line up with the field, while the AFM spins remain random. (i).

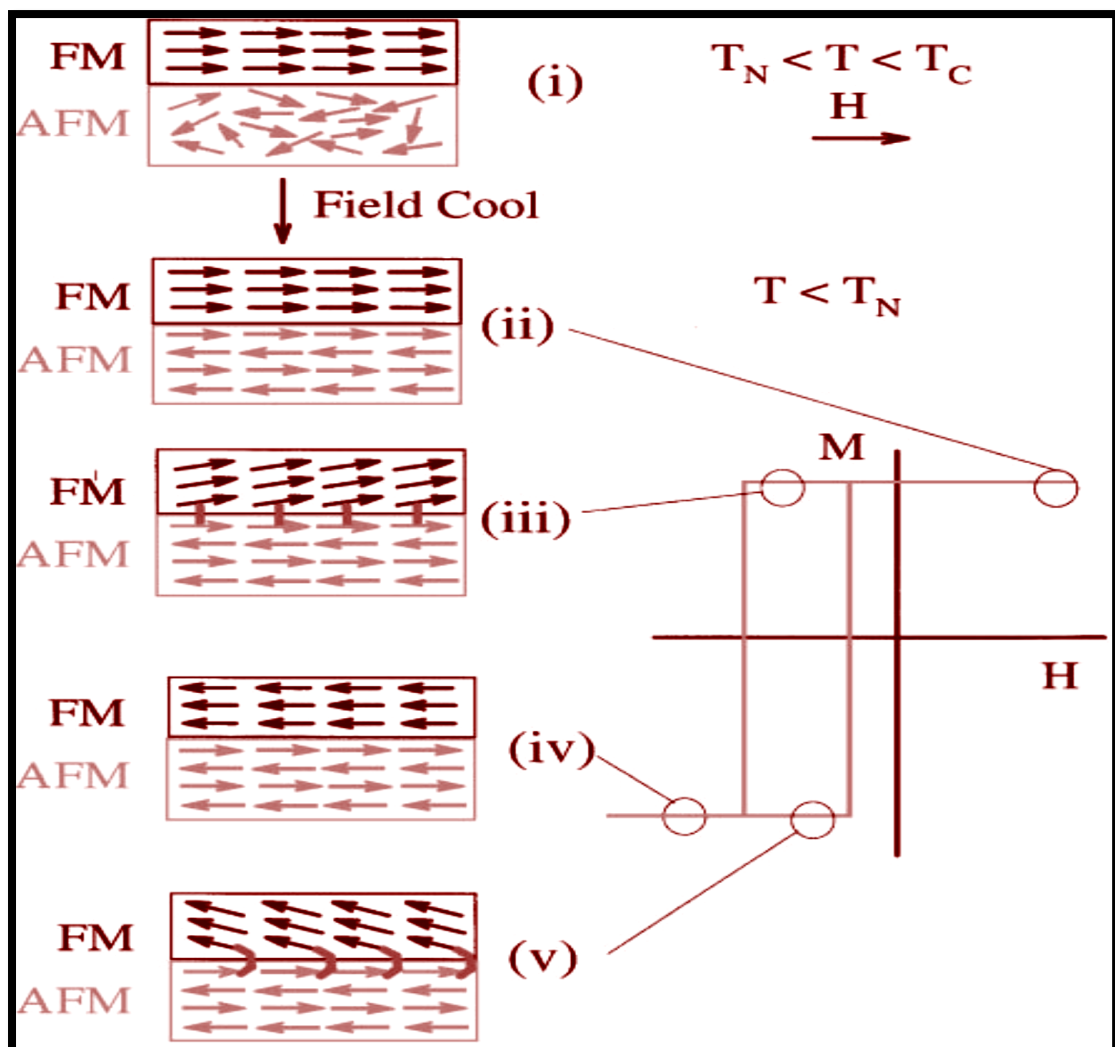


Fig.1.19. Schematic diagram of the spin configuration of an FM-AFM bilayer (a) at different stages (i)-(v) of an exchange biased hysteresis loop (b). (Courtesy: J. Nogues et. al, JMMM 192,203,1999)[100]

In the presence of the field, due to the interaction at the interface as cooling to $T < T_N$, the AFM spins next to the FM align ferromagnetically to those of the FM. The other spin planes in the AFM follow the AFM order so as to produce zero net magnetization. (ii). When the field is reversed, the FM spins start to rotate. However, for sufficiently large AFM anisotropy, the AFM spins remain unchanged. (iii). The interfacial interaction between the FM-AFM spins at the interface, tries to align ferromagnetically the FM spins with the AFM spins at the interface. Moreover, AFM spins at the interface exert a small torque on the FM spins, to maintain their original

position. FM spins have single stable configuration, so that the anisotropy is unidirectional. Thus the field needed to reverse completely an FM layer will be larger if it is in contact with an AFM. It is due to the fact that an extra field is needed to overcome to the microscopic torque (ii). However, once the field is rotated back to its original direction, the FM spins will start to rotate at a smaller field, due to the interaction with the AFM spins. (v and ii). The material behaves as if there was an extra (biasing field), therefore, the FM hysteresis loop is shifted in the field axis, i.e. exchange bias.

1.2.8 .1 The ideal Meiklejohn-Bean model:

The first theoretical approach which explain the EB effect was the model proposed by Meiklejohn and Bean [101]. According to this model, change into the magnitude of the hysteresis shift of the FM/AFM systems. The following assumptions are made in the Meiklejohn and Bean model [102]: The FM is in a single domain state and rotates rigidly. The AFM, having an in-plane uniaxial anisotropy, is also in a single domain state and the orientation of the AFM spins remains unchanged during the rotation of the FM spins. The exchange interaction across the FM/AFM interface is characterized by the interfacial exchange coupling energy per unit area, J_{EB} . The Stoner-Wohlfarth model [103] was used for describing the coherent rotation of the magnetization vector of the FM. Fig. 2.3 shows the geometry of the vectors involved in the Meiklejohn and Bean model. H is the applied magnetic field, which makes an angle θ with respect to the field cooling direction denoted by $\theta = 0$. K_{FM} and K_{AFM} are the uniaxial anisotropy directions of the FM and the AFM layer, respectively.

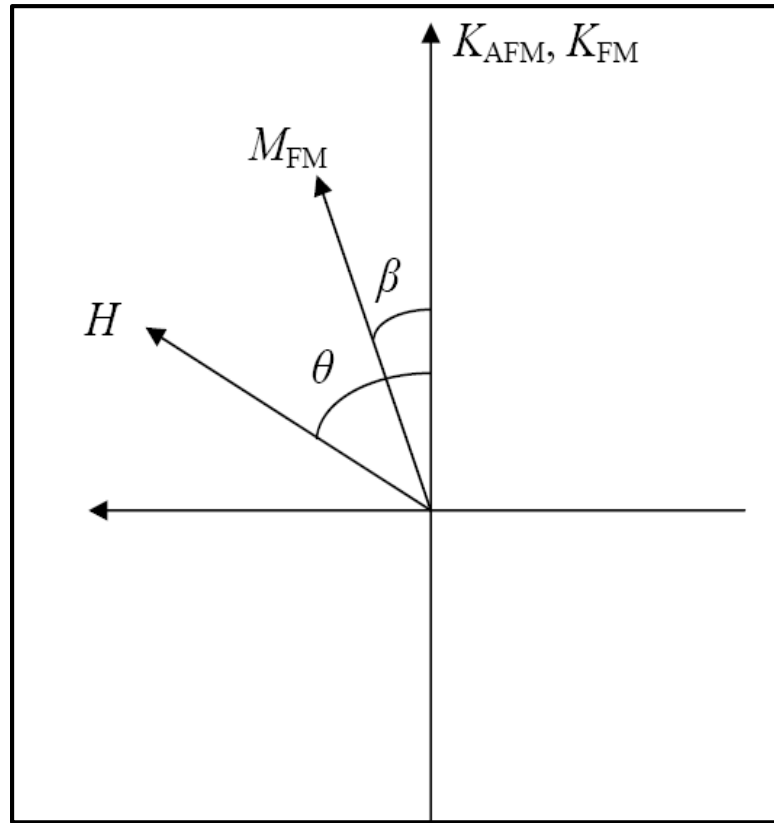


Fig. 1.20. Schematic view of the angles and vectors used in the Meiklejohn and Bean model. (Courtesy: J.Nogues et. al, JMMM 192,203,1999)[100]

Under these assumptions the energy per unit area considering coherent rotation of magnetization can be written as :

$$E_A = -\mu_0 H M_{FM} t_{FM} \cos(\theta - \beta) + K_{FM} t_{FM} \sin^2 \beta - J_{EB} \cos \beta$$

The interfacial exchange energy can be further expressed in terms of pair

exchange interactions: $E_{int} = \sum_{i,j} J_{ij} S_i^{AFM} S_j^{FM}$

where the summation includes all interactions within the range of the exchange coupling [36].

The stability condition: $\frac{\delta E_A}{\delta \beta} = 0$

has two types of solutions. One is

$$\beta = \cos^{-1} \left[\frac{(J_{EB} - \mu_0 H M_{FM} t_{FM})}{(2K_{FM})} \right] \text{ for } \mu_0 H M_{FM} t_{FM} - J_{EB} \leq 2K_{FM}$$

The other one is $\beta = 0, \pi$ for $\mu_0 H M_{FM} t_{FM} - J_{EB} \geq 2K_{FM}$

corresponding to positive and negative saturation, respectively. The coercive fields H_{C1} and H_{C2} are extracted from the stability equation above for $\beta = 0, \pi$:

$$H_{C1} = -\frac{2K_{FM}t_{FM} + J_{EB}}{\mu_0 M_{FM}t_{FM}}$$

$$H_{C2} = \frac{2K_{FM}t_{FM} - J_{EB}}{\mu_0 M_{FM}t_{FM}}$$

The coercive field H_C of the loop and the EB field H_{EB} can be calculated according to:

$$H_C = \frac{-H_{C1} + H_{C2}}{2} \quad \text{and} \quad H_{EB} = \frac{H_{C1} + H_{C2}}{2}$$

which further gives:

$$H_C = \frac{2K_{FM}}{\mu_0 M_{FM}}$$

$$H_{EB} = -\frac{J_{EB}}{\mu_0 M_{FM}t_{FM}}$$

Above equation gives the expression of the EB field according to the Meiklejohn and Bean model. This equation predicts that the sign of the exchange bias is negative with respect to the cooling field direction. Almost all hysteresis loops shown in the literature are shifted oppositely to the field cooling direction. Positive exchange bias was observed for instance in CoO/Co, $\text{Fe}_x\text{Zn}_{1-x}\text{F}_2/\text{Co}$ and $\text{Cu}_{1-x}\text{Mn}_x/\text{Co}$ bilayers when the measurement temperature was close to the blocking temperature.

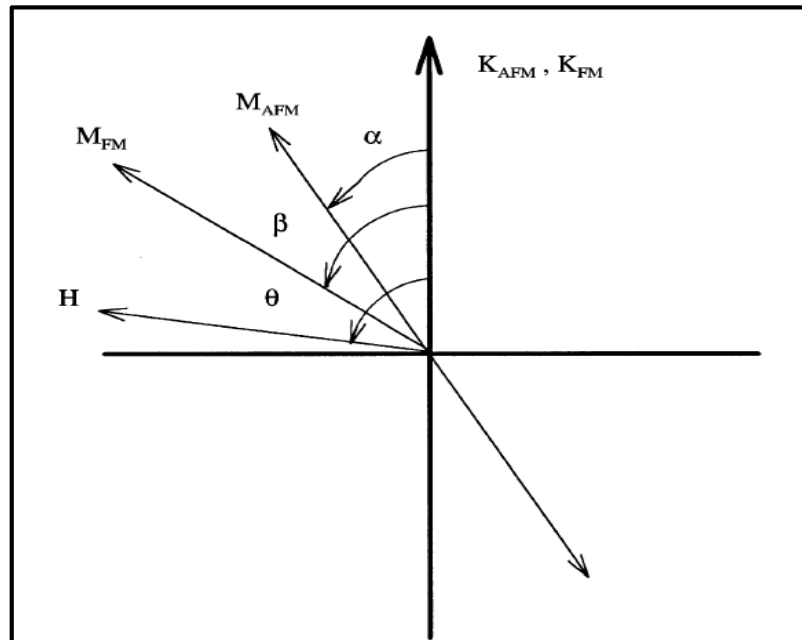


Fig.1.21. Schematic diagram of angles involved in an exchange bias system. Note that the AFM and FM anisotropy axes are assumed collinear and that the AFM sublattice magnetization M_{AFM} has two opposite directions. (Courtesy: J.Nogues et. al, JMMM 192,203,1999)[100]

$$E = -HM_{\text{FM}}t_{\text{FM}}\cos(\theta - \beta) + K_{\text{FM}}t_{\text{FM}}\sin^2\beta + K_{\text{AFM}}t_{\text{AFM}}\sin^2\alpha - J_{\text{INT}}\cos(\beta - \alpha)$$

where H is the applied field, M_{FM} the saturation magnetization, t_{FM} the thickness of the FM layer, t_{AFM} the thickness of the AFM layer, K_{FM} the anisotropy of the FM layer, K_{AFM} the anisotropy of the AFM layer and J_{INT} the interface coupling constant. β , α and θ are the angles between the magnetization and the FM anisotropy axis, the AFM sublattice magnetization (M_{FM}) and the AFM anisotropy axis, and the applied field and the FM anisotropy axis. The first term in the energy equation accounts for the effect of the applied field on the FM layer, the second term is the effect of the FM anisotropy, the third term takes into account the AFM anisotropy and the last term takes into consideration the interface coupling. If

$$K_{\text{FM}}t_{\text{FM}} \leq K_{\text{AFM}}t_{\text{AFM}}$$

thus the energy becomes

$$E = -HM_{\text{FM}}t_{\text{FM}}\cos(\theta - \beta) + K_{\text{AFM}}t_{\text{AFM}}\sin^2\alpha - J_{\text{INT}}\cos(\beta - \alpha)$$

Minimizing the energy with respect to α and β the loop shift is found to be

$$H_E = \frac{J_{\text{INT}}}{M_{\text{FM}}t_{\text{FM}}}$$

$K_{\text{AFM}}t_{\text{AFM}} \geq J_{\text{INT}}$ is required for the observation of exchange anisotropy. $K_{\text{AFM}}t_{\text{AFM}} \geq J_{\text{INT}}$ then the system is minimized by keeping α small independently of β . However if $J_{\text{INT}} \geq K_{\text{AFM}}t_{\text{AFM}}$, AFM and FM spins rotate together.

1.2.6.2 Training effect: It is well known that in many exchange-biased systems, H_E depends on the number of measurements, a property often called a training effect. This effect comprises the reduction of H_{EB} and H_C with consecutive hysteresis loops at a fixed temperature: $H_{\text{EB}}(\text{1st loop}) > H_{\text{EB}}(\text{2nd loop}) > \dots > H_{\text{EB}}(\text{nth loop})$. It has been suggested that two types of training effect are present in EB systems, one between the first and second loop and another one involving subsequent higher number of loops. The first type of training effect has been proposed to arise from the AFM magnetic symmetry. For the second type of training effect, it has been demonstrated experimentally that, in thin film systems, the reduction of H_{EB} is proportional to the number of loops $H_{\text{EB}} \sim n^{-1/2}$ (for $n > 2$), where n is the number of loops carried out. The relationship between H_E and loop index n can be expressed by power law:

$$H_E - H_\infty = \frac{k}{\sqrt{n}}$$

Here, H_E is the exchange bias field in the limit of infinite loops and k is the sample-dependent constant. Recently, Binek et al. considered the training effect in FM/AFM heterostructures in the framework of nonequilibrium thermodynamics. It was proposed that consecutively cycled hysteresis loops of the FM layer could cause the spin configurational relaxation of the AFM interface magnetization toward equilibrium and the corresponding formula can be obtained describing loop index n which dependent on H_E is expressed as

$$H_E(n+1) - H_E(n) = -\gamma_H [H_E(n) - H_E(\infty)]^3$$

where γ_H is a sample-dependent constant and $H_E(\infty)$ is the exchange bias field in the limit of infinite loops.

1.2.9 Spin Glass :

In class of spin glass system ,the magnetic moments exist in frozen random arrangements. Its state was defined as a random, mixed-interacting magnetic system characterized by a random, cooperative, freezing of spins at a well defined temperature T_f below this temperature , it shows highly irreversible, metastable frozen state without the usual magnetic long range ordering [96]. Different parts of this definition in much more detail given as: Site-randomness: A commonly studied spin glass is $\text{Cu}_{1-x}\text{Mn}_x$ with $x \leq 1$ in which incorporation of small amounts of Mn into the Cu matrix occurs completely randomly with no shortrange ordering. This directly leads to a random distance between magnetic Mn ions in the non-magnetic Cu matrix. Bond-randomness: In this randomness ,the nearest neighbor interactions vary between $+J$ and $-J$. The randomness inherent in a spin glass is important, but equally important is the presence of competing interactions .The distribution of distances between moments in a random-site spin glass leads to competing interactions because the interactions are of RKKY-type $[J_{\text{RKKY}} \propto \frac{\text{Cos}(2K_F r)}{r^3}$, where J_{RKKY} denotes the coupling of an r - dependent exchange interaction, and K_F is radius of spherical fermi surface. The interaction is long range and has an oscillatory dependance on the distance between the magnetic moments. Hence depending on the seperation it may be either ferromagnetic or antiferromagnetic and therefore their sign (ferromagnetic or

antiferromagnetic) depends on the distance between the spins. Another contributing feature is the magnetic anisotropy, due to single-ion anisotropy or Dzyaloshinsky-Moriya interactions [when acting between two spins S_1 and S_2 and its Hamiltonian $\overrightarrow{H_{DM}} = D \cdot S_1 \times S_2$ where vector D vanishes when the crystal field has an inversion symmetry with respect to the centre between the two magnetic ions. In general D may not vanish and will lie parallel or perpendicular to the line connecting the two spins, depending on the symmetry. At high temperature the behaviour of all magnetic systems is dominated by thermal fluctuations, so that in a spin glass all the spins are independent. As a spin glass is cooled from high temperature, the independent spins slow down and build up into locally correlated units, known as clusters. The spins which are not in clusters take part in interactions between clusters. As the temperature cools to T_f the fluctuations in the clusters progressively slow down. The interactions between spins become more long range so that each spin becomes more aware of spins in a progressively growing region around it. This mechanism is not fully understood and it seems to be a cooperative phase transition. Below T_f the ground state appears to be 'glassy', possessing metastability and slow relaxation behaviour. One of the signatures of spin glass behaviour is a sharp peak close to T_f in the real part of the a.c. susceptibility, $\chi(\omega)$. In this technique the magnetic susceptibility is measured using a very small alternating magnetic field of frequency ω , sometimes with a constant (d.c.) magnetic field also applied. The position of the peak varies slightly with ω . The imaginary part of $\chi(\omega)$, related to the absorption, shows a sudden onset near T_f . The dynamics of the fluctuations associated with the freezing process can be studied using a.c. susceptibility. A criterion which is often used to compare the frequency dependence of T_f in different spin-glass systems is to compare the relative shift in freezing temperature per decade of frequency, [104]

$$\delta T_f = \frac{\Delta T_f}{T_f \Delta(\log_{10} \nu)}$$

The frequency dependence of T_f follows the conventional power law divergence of critical slowing down,

$$\tau = \tau_0 \left(\frac{T_f - T_{SG}}{T_{SG}} \right)^{-z\nu'}$$

where τ is the relaxation time corresponding to the measured frequency ($\tau = 1/\nu$), τ_0 is the characteristic relaxation time of single spin-flip, T_{SG} is the spin glass temperature as frequency tends to zero, and $z\nu'$ is the dynamic critical exponent and ν' is the critical exponent of correlation length,

$$\xi = \left(\frac{T_f}{T_{SG}} - 1\right)^{-\nu'}$$

and the dynamical scaling relates τ to ξ as $\tau \sim \xi^z$. For a spin-glass system the critical exponent $4 \ll z\nu' \ll 12$. It is useful to rewrite

$$\log(\tau) = \log(\tau_0) - z\nu' \log(t),$$

where $t = \left(\frac{T_f}{T_{SG}} - 1\right)$. The slope and intercept of $\log(\tau)$ vs $\log(t)$ plot can thus be used to estimate τ_0 and $z\nu'$. A log-log plot of inverse frequency (τ) vs. reduced temperature (t). The value of T_{SG} was determined by extrapolating the T_f vs. ν plot to $\nu = 0$, which gives T_{SG} and fit to the power law divergence, find the value of τ_0 and $z\nu'$.

Arrhenius law: The presence of interacting clusters is also evident from the departure of frequency dependence of T_f from the

$$\nu = \nu_0 \exp\left(-\frac{E_a}{K_B T_f}\right)$$

where k_B is the Boltzmann constant, ν_0 is the characteristic attempt frequency and E_a is the average thermal activation energy. According to this law one would expect a linear behavior in a plot of $\ln(\nu)$ against $1/T_f$. It can be seen from the $\ln(\nu)$ vs. $1/T_f$ plot that there is significant deviation from the expected linear behavior at low frequencies, implying that the dynamics is not simply associated with the single-spin flips, rather reflects a cooperative character of the freezing.

Vogel- Fulcher law: Frequency dependence of freezing temperature T_f when fitted to the empirical, [105]

$$\nu = \nu_0 \exp\left(-\frac{E_a}{K_B (T_f - T_0)}\right)$$

With three fitting parameters the characteristic attempt frequency ν_0 , the activation energy E_a , and the Vogel- Fulcher temperature T_0 which is often interpreted as a measure of inter cluster interaction strength gives a reasonable estimate of activation energy. In order to estimate the fitting parameters ν_0 , E_a , and T_0 in two different ways, both of which gave consistent values of these parameters.

$$\ln\left(\frac{\nu_0}{\nu}\right) = \frac{E_a}{k_B(T_f - T_0)}$$

or

$$T_f = \frac{\frac{E_a}{k_B}}{\ln\left(\frac{\nu_0}{\nu}\right)} + T_0$$

Thus E_a/k_B and T_0 can be obtained from the slope and intercept of T_f vs $1/\ln(\nu_0/\nu)$ plot. A plot of T_f vs. $100/\ln(\nu_0/\nu)$ together with the fit to Vogel-Fulcher law.

In order to ensure about the appropriate parameters as a consequence of fixing the attempt frequency ν_0 , the value of Vogel-Fulcher temperature T_0 by following the method suggested by **Souletie and Tholence**[106]

$$\ln(\nu) = \ln(\nu_0) - \frac{\frac{E_a}{k_B}}{(T_f - T_0)}$$

which would then allow us to estimate E_a/k_B and τ_0 from the slope and intercept of $\ln(\nu)$ vs $\frac{1}{(T_f - T_0)}$ plot, respectively. A linear fit to $\ln(\nu)$ vs $\frac{1}{(T_f - T_0)}$ plot gives characteristic relaxation time, τ_0 and activation energy E_a/k_B . Isothermal remanent magnetizations $M_{IRM}(t)$ were measured at different magnetic fields after the ZFC process from 300 to 5 K. It is worth noting that the sample was first zero-field cooled to the desired temperature, and then a magnetic field was applied for about 600s. After switching off the magnetic field, the remanent magnetization was measured as a function of time. $M_{IRM}(t)$ decays so slowly that its value is nonzero even after several hours of decay, which is also a fingerprint of SG behavior.

$$M_{IRM}(t) = M_0 - \alpha \ln(t)$$

Fitting parameters M_0 and α as a function of magnetic field are plotted, and both values increase initially and then saturate, which has been observed in several different SG systems and can be ascribed to the existence of spin frustration.

1.2.8 Griffith Phase:

The Griffiths model:

According to the Landau theory of phase transitions, the phase state of a system is characterized by the order parameter Φ ($\Phi = 0$ in the disordered phase and $\Phi \neq 0$ in an ordered phase). It is postulated that near the phase transition point T_C , the static characteristics of all systems behave in similar fashion. If phase transitions assumes

that the system is homogeneous, i.e., there is a single transition temperature T_C for the entire system. This condition is clearly not satisfied in disordered systems, for example, in magnets where part of the magnetic bonds are absent. In that case the transition temperature T_C can be different for different regions of the system, i.e. $T \rightarrow T_C(x)$. Griffith was first examined in such magnetic system in which part of the magnetic bonds (or magnetic ions) are absent. Fig1 is a schematic illustration of a ferromagnet in which magnetic ions are missing at lattice sites. The absence of magnetic ions weakens the tendency of the system to form a magnetically ordered state and the temperature at which the entire system transforms to an ordered state will be lower than the temperature T_C^0 for an ideal system.

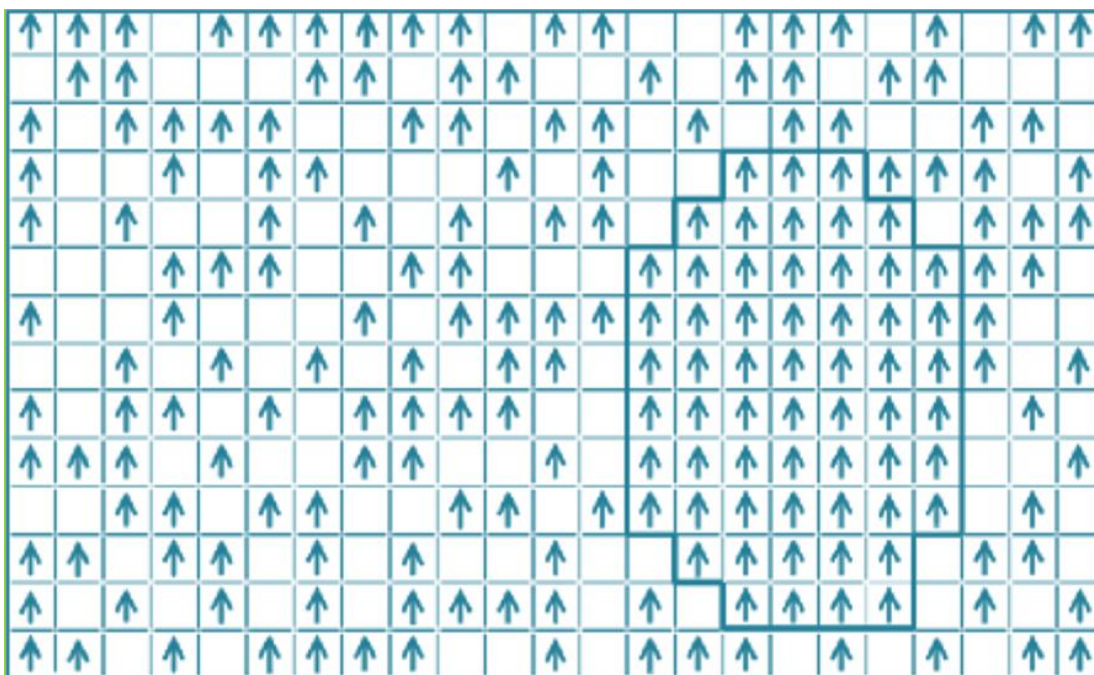


Fig.1.22. A schematic illustration of a diluted ferromagnet in which magnetic ions are missing at some lattice sites. A region in which all the magnetic ion sites are occupied is outlined. (Courtesy: V. N. Krivoruchko, *Low Temperature Physics*40, 586 ,2014)[107]

In addition, in an infinite system (the thermodynamic limit) there is always a large cluster (indicated in Fig. 1) which goes into an ordered state for $T < T_C^0$ while the rest of the system will remain in a disordered state. The transition of the cluster into an ordered state cannot be treated as the formation of a nucleus of a new phase. At the same time, the existence of the magnetically ordered phase can be established on the

basis of its characteristic resonance response(fig esr) Thus, in a magnet with some of the magnetic bonds missing, a new phase appears above the Curie temperature T_C of the entire system but below some temperature T_G (corresponding to the Curie temperature of the ideal system); this new phase consists of ferromagnetic clusters in a paramagnetic matrix. Since publication of the papers by *Bray and Moore [108]*, this phase has been referred to as the Griffiths phase.

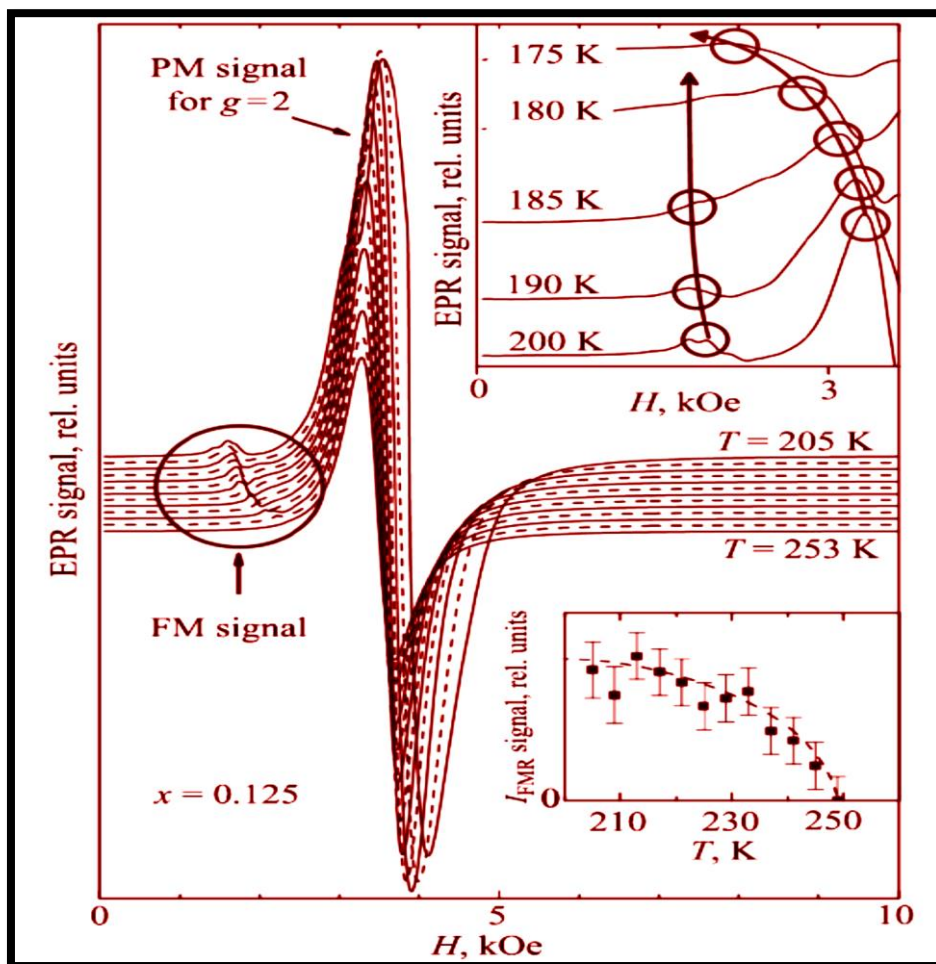


Fig.1.23. ESR spectra for $x = 0.125$ for $205 \ll T \ll 253$ with the magnetic field applied within the easy ac plane. Upper inset: Evolution of the spectra towards T_C . Lower inset: T dependence of the FMR intensity. (Courtesy: J. Deisenhofer, et.al, *Phys RevLett.*95, 257202, 2005)[109]

1.2.8.1 Critical behavior of the ferromagnetic in the Griffiths phase:

Landau theory of phase transitions, the free energy of a system near the ferromagnetic-paramagnetic transition can be expressed as

$$G(\mathbf{M}, \mathbf{T}) = G_0 + \frac{1}{2}A(\mathbf{T}-T_c)M^2 + \frac{1}{4}BM^4 + \frac{1}{2}CM^6 - MH,$$

where $A > 0$ and $C > 0$.

Minimising equation, we obtain

$$\frac{H}{M} = A(\mathbf{T} - T_c) + BM^2 + CM^4$$

In the case of first order phase transition, i.e. $B < 0$. Then the constant B determines the slope of the $\frac{H}{M} = f(M^2)$ curves (**Belov-Arrott isotherms**). While the derivative $\frac{dM}{dH}$ has a maximum.

In the case of second order phase transition, i.e. for $B > 0$, the isotherms are monotonic. If the transition into the ferromagnetic phase takes place in a magnet for which the magnetic bond between may be absent with a probability of $(1-p)$, then system is in neither a paramagnetic nor a ferromagnetic state in temperature range $T_c(p) < T < T_c$. The free energy of the system will be a nonanalytic function of field over the entire temperature range $T_c(p) < T < T_c$ (the temperature interval within which the Griffiths phase exists). Paramagnetic-Ferromagnetic second order phase transition is characterized by the following set of scaling relations:

$$M \propto m_0 |\tau|^\beta, \quad \tau \geq 0,$$

$$\chi_0 \propto \frac{1}{|\tau|^\gamma}, \quad \tau \leq 0,$$

$$M \propto H^{\frac{1}{\delta}}, \quad \tau = 0$$

where $\tau = \frac{(T-T_c)}{T_c}$ and the critical indices $\beta, \gamma,$ and δ describes the following dependences: β , the spontaneous magnetization M as a function of temperature γ , the static susceptibility, χ_0 as a function of temperature for $H=0$, and δ , the magnetization as a function of magnetic field at T_c .

1.2.9 Transport Properties:

1.2.9.1 Variable Range Hopping:

Delafossites CuCrO_2 and Credenerite CuMnO_2 are insulators and semiconductor. The electrical transport in these materials is thermally activated and Variable Range Hopping (VRH) model is one of the physical models that can describe the

temperature dependence of the conductivity in the insulating system. Sir Nevill Mott [110] proposed VRH model to describe the behavior of the resistivity in systems with disorder and at low temperature.

Suppose we have two states in which their distance is r and they are localized, if the first state has energy E_1 and the second state has energy E_2 and the energy difference $W = E_2 - E_1 > 0$ then the electron can jump from the first state to the second state by absorbing a phonon. If μ_1 and μ_2 are the electric potential energy of the first state and second state, then the current is given by

$$I = \frac{er\omega_0}{k_B T} (\mu_1 - \mu_2) \exp(-W/k_B T) \exp(-2r/\xi),$$

By taking $\mu_1 - \mu_2 = eV$, the resistance can be evaluated as

$$R = \frac{k_B T}{e^2 r \omega_0} (\exp(-W / k_B T) \exp(-2r/\xi))^{-1}$$

where ω_0 is a frequency from typical phonon and ξ is the localization length. The conductivity can be written

$$\sigma = \sigma_0 \exp\left(-\frac{2r}{\xi} - \frac{W}{k_B T}\right)$$

For $d = 3$, the density $N\{E\}$ is given by

$$N\{E\} = \frac{3}{4\pi r^3 W}$$

$$W = \frac{3}{4\pi r^3 N\{E\}},$$

where $N\{E\}$ is the density of states.

Solve equation and maximizing σ by taking its derivative = 0, we obtain

$$r = \left(\frac{9\xi}{8\pi N\{E\}k_B}\right)^{\frac{1}{4}} \left(\frac{1}{T}\right)^{\frac{1}{4}}$$

Substituting equation (1.23) into equation (1.20) and finally we obtain

$$\sigma = \sigma_0 \exp[-(T_0/T)^{0.25}]$$

which implies

$$\rho(T) = \rho_0 \exp(T_0/T)^{0.25}$$

where T_0 is the characteristic barrier energy parameter and it can be calculated from the slope of $\ln \rho$ versus $(1/T)^{0.25}$ curve (Fig. 1.13 (a)). Finally, we obtain the relation between the barrier energy parameter T_0 and the localization length ξ solve equation and evaluate for T_0 , we obtain

$$T_0 \propto \frac{1}{N\{E\}\xi^3},$$

Localization length is a characteristic of a localized system where the smaller ξ is, the more localized the system. A physical interpretation of the localization length in a localized system is illustrated in Fig. 1.13 (b)

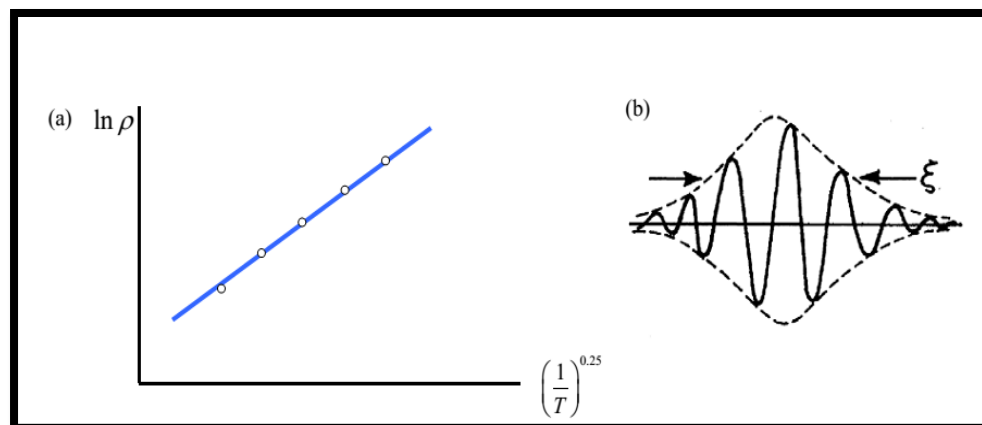


Fig. 1.24. (a) $\ln \rho$ versus $(1/T)^{0.25}$ from VRH model, the barrier energy parameter T_0 is calculated from the slope of the curve. (b) The localization length in the localized wave function (from reference [70])

1.2.9.2 Arrhenius law:

Arrhenius equation was proposed by Dutch chemist, J.H van't Hoff in 1884. However, Svante Arrhenius was the first person who gave the physical interpretation of this equation. He was using this equation to explain the dependence of the rate constant k of a chemical reaction on the activation energy E_a and temperature T .

$$k = A \exp(-E_a / RT),$$

where R is a gas constant. In general, many thermally activated processes can be evaluated by using Arrhenius law. In the electrical transport mechanism, the

resistance of a semiconducting or an insulating material can also be explained by using this model and we can express the resistance (resistivity) as following

$$\mathbf{R = R_0 \exp(E_a / k_B T) ,}$$

here, k_B is the Boltzmann constant and E_a is the activation energy and can be obtained from the slope of $\ln \rho$ versus $(1/T)$ curve (Fig. 1.14 (a)).

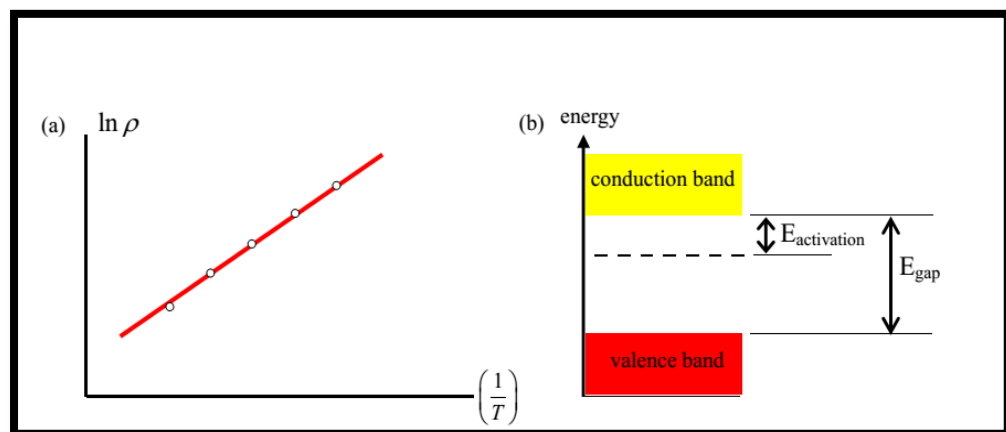


Fig.1.25 (a) $\ln \rho$ versus $(1/T)$ from Arrhenius model. (b) The activation energy and the band gap between valence and conduction bands.

1.2.9.3 The Modified Arrott Plot:

The modified Arrott plot can be used in order to study the critical spin fluctuations near the ferromagnetic transition, by analyzing the spontaneous magnetization M_s and the inverse of the initial χ_0^{-1} susceptibility. Arrott plot was originated from the Landau theory of the second order ferromagnetic phase transition. Before the modified Arrott plot, there was a plot called Arrott plot proposed by A. Arrott. In general, this plot is non linear and there is a difficulty to determine accurately the value of M_s , χ_0^{-1} . However, Anthony Arrott and John E. Noakes then suggested a more practical and powerful plot and is known as the modified Arrott plot [109]. In the modified Arrott plot, in which the $M_s^{1/\beta}$ versus $(H/M)^{1/\gamma}$ from the M-H data around the transition temperature. This plot yields a set of parallel straight lines near T_c . The relations of the spontaneous magnetization M_s and the inverse of the initial susceptibility χ_0^{-1} are given by

$$(\chi_0)^{-1}(T) \propto (T - T_c)^\gamma, \text{ for } T > T_c$$

$$\mathbf{H} \propto \mathbf{M}^\delta, \text{ for } T = T_c \text{ and}$$

$$\mathbf{M}_s(T) \propto (T_c - T)^\beta$$

From the Arrott plot, we can see if a system obeys the Ising model or Heisenberg model or the Molecular Field Theory.

Motivation and Importance of the studied systems:

- Geometrically frustrated magnetic systems have attracted much attention because of their tremendous magnetic properties.
- AFM–FM behavior, Geometric frustration observed in Crednerite CuMnO_2 , and Delafossite CuCrO_2 system.
- Exchange bias, Spin glass and Griffith phase should exist in such type of layered structure.
- Type-II multiferroics are very promising from application point of view. Cycloidal spiral type structure is found in CuCrO_2 system which leads to multiferroic behavior.
- In case of CuMnO_2 , its structure is Crednerite which is distorted form of Delafossite structure. Hence there is enormous possibility of getting unconventional type of magnetic ordering such as spin glass, Griffith phase, exchange bias etc.
- In CuCrO_2 system, frustration arises due to its Delafossite structure which leads to magneto electric coupling which has several practical applications like sensitive detection of magnetic field, advanced logic devices and tunable devices.

References:

- [1] Karmakar, A., Majumdar, S., Kundu, S., Nath, T.K., and Giri, S., A Griffiths-like phase in antiferromagnetic $R_{0.5}Eu_{0.5}MnO_3$ ($R = Pr, Nd, Sm$), *J. Phys.: Condens. Matter* 25, 066006. (2013)
- [2] Perez, N., Casanova, F., Luis, F.B., Garcia, M., Labarta, A., and X. Batlle, Griffiths-like phase and magnetic correlations at high fields in Gd_5Ge_4 . *Phys. Rev. B* 83, 184411 (2011)
- [3] Albillos, J.H., Miguel Garcia L., and Bartolome, F., Observation of a Griffiths-like phase in the paramagnetic regime of $ErCo_2$. *J. Phys.: Condens. Matter* 21, 216004 (2009)
- [4] Ghosh, K., Chandan Mazumdar, C., Ranganathan, R., and Mukherjee, S., Griffiths phase behaviour in a frustrated antiferromagnetic intermetallic compound; *Nature scientific reports* 5, 15801 (2015).
- [5] Chatterjee, S., and Nigam, A.K., Spin-glass-like behavior in $Y_{1-x}Sr_xMnO_3$ ($x=0.5$ and 0.6), *Phys. Rev. B* 66, 104403 (2002).
- [6] Lin, S., Shao, D. F., Lin, J. C., Zu, L., Kan, X. C., Wang, B. S., Huang, Y. N., Song, W. H., Lu, W. J., Tong, P., and Y. P. Sun., Spin-glass behavior and zero-field-cooled exchange bias in a Cr-based antiperovskite compound $PdNCr_3$. *Mater. Chem. C*, 2015, 3, 5683
- [7] Nam, D. N. H., Mathieu, R., Nordblad, P., Khiem, N. V., Phuc, N. X., Spin-glass dynamics of $La_{0.95}Sr_{0.05}CoO_3$. *Phys. Rev. B* 62, 8989, (2000).
- [8] Arkenbout, A. H., Palstra, T. T. M., Siegrist, T., and Kimura, T., Ferroelectricity in the cycloidal spiral magnetic phase of $MnWO_4$. *Phys. Rev. B* 74, 184431 (2006)
- [9] Chowki, S., Basu, T., Singh, K., Mohapatra, N., and Sampathkumar, E. V., Multiferroicity and magneto-electric effect in Gd_2BaNiO_5 , *J. Appl. Phys.* 115, 214107 (2014)
- [10] Basu, T., Singh, K., S. Gohil, S. Ghosh, and E. V. Sampathkumar, Implications of magnetic and magnetodielectric behavior of $GdCrTiO_5$. *J. Appl. Phys.* 118, 234103 (2015)
- [11] Fang, Y., Song, Y. Q., Zhou, W. P., Zhao, R., Tang, R. J., H. Yang, L. Y. L., Yang, S. G., Wang, D. H. and Du, Y. W., Large magnetoelectric coupling in $Co_4Nb_2O_9$.
- [12] Li, D., X. Fang, Zanhong Deng, Shu Zhou, Ruhua Tao, Weiwei Dong, Tao Wang, Yiping Zhao, Gang Meng and Xuebin Zhu; Electrical, optical and structural properties of $CuCrO_2$ films prepared by pulsed laser deposition; *J. Phys. D: Appl. Phys.* 40 (2007) 4910–4915

-
- [13] Pachoud, E., Singh, K., Y. Breard, C. Martin, G. Andre V. Hardy, Ch. Simon, and A. Maignan., Magnetic dilution and steric effects in the multiferroic delafossite CuCrO_2 . *Phys. Rev. B* 86, 054437 (2012).
- [14] Kimura, K., Nakamura, H., S. Kimura, M. Hagiwara, and T. Kimura., Tuning Ferroelectric Polarization Reversal by Electric and Magnetic Fields in CuCrO_2 . *Phys. Rev. Lett.* 103, 107201 (2009)
- [15] Mun, E., M. Frontzek, A. Podlesnyak, G. Ehlers, S. Barilo, S. V. Shiryayev, and Vivien S. Zapf., High magnetic field evolution of ferroelectricity in CuCrO_2 . *Phys. Rev. B* 89, 054411 (2014)
- [16] Aktas, O., Quirion, G., T. Otani, and T. Kimura; First-order ferroelastic transition in a magnetoelectric multiferroic: CuCrO_2 , *Phys. Rev. B* 88, 224104 (2013)
- [17] Aoyama, T., Atsushi Miyake, Tomoko Kagayama, Katsuya Shimizu, and Tsuyoshi Kimura., Pressure effects on the magnetoelectric properties of a multiferroic triangular-lattice antiferromagnet CuCrO_2 . *Phys. Rev. B* 87, 094401 (2013).
- [18] Kimura, K., H. Nakamura, Kenya Ohgushi, and Tsuyoshi Kimura., Magnetoelectric control of spin-chiral ferroelectric domains in a triangular lattice antiferromagnet., *Phys. Rev. B* 78, 140401 (2008).
- [19] Poienar, M., Damay, F. Martin, C., J. Robert, and S. Petit, Spin dynamics in the geometrically frustrated multiferroic CuCrO_2 . *Phys. Rev. B* 81, 104411 (2010).
- [20] Meng, Q., Shanfu Lu, Sunhui Lu and Yan Xiang; Preparation of p-type $\text{CuCr}_{1-x}\text{Mg}_x\text{O}_2$ bulk with improved thermoelectric properties by sol-gel method; *J Sol-Gel Sci Technol.* 63, 1-7 (2012)
- [21] Singh, K., Antoine Maignan, Charles Simon, Sanjay Kumar, Christine Martin, O. Lebedev, Stuart Turner and G. Van Tendeloo., Magnetodielectric $\text{CuCr}_{0.5}\text{V}_{0.5}\text{O}_2$: an example of a magnetic and dielectric multiglass., *J. Phys.: Condens. Matter* 24 (2012) 226002.
- [22] Frontzek, M., G Ehlers, A Podlesnyak, H Cao, M Matsuda, O Zaharko, N Aliouane, S Barilo and S V Shiryayev., Magnetic structure of CuCrO_2 : a single crystal neutron diffraction study. *J. Phys.: Condens. Matter* (2012) 016004.
- [23] Barton, P.T., Ram Seshadri, Andrea Knoller and Matthew J Rosseinsky, Structural and magnetic characterization of the complete delafossite solid solution $(\text{CuAlO}_2)_{1-x}(\text{CuCrO}_2)_x$; *J. Phys.: Condens. Matter* 24 (2012) 016002.
- [24] Luo, S., Wang, K. F., Li, S. Z., Dong, X. W., Yan, Z. B., Cai, H. L., and J.M. Liu Enhanced ferromagnetism and ferroelectricity in multiferroic $\text{CuCr}_{1-x}\text{Ni}_x\text{O}_2$., *Applied Physics Letters* 94, 172504 (2009).

-
- [25] Ngo, T. N. M., Adem, U. and T. T. M. Palstra., The origin of thermally stimulated depolarization currents in multiferroic CuCrO_2 Appl. Phys. Lett. 106, 152904 (2015).
- [26] Terada, N., Dmitry D. Khalyavin, Pascal Manuel, Yoshihiro Tsujimoto, Kevin Knight, Paolo G. Radaelli, Hiroyuki S. Suzuki, and Hideaki Kitazawa., Spiral-Spin-Driven Ferroelectricity in a Multiferroic Delafossite AgFeO_2 , Phys. Rev. Lett. 109, 097203 (2012).
- [27] Nakajima, T. and Setsuo Mitsuda., Magnetic interactions in the multiferroic phase of $\text{CuFe}_{1-x}\text{Ga}_x\text{O}_2$ ($x=0.035$) refined by inelastic neutron scattering with uniaxial-pressure control of domain structure, Phys. Rev. B 85, 144405 (2012).
- [28] Pavunny, S. P., A. Kumar, and R. S. Katiyar., Raman spectroscopy and field emission characterization of delafossite CuFeO_2 ; J. Appl. Phys. 107, 013522 (2010)
- [29] Zhong, C., Haixia Cao, Jinghui Fang, Xuefan Jiang, Xianming Ji., Spin-lattice coupling and helical-spin driven ferroelectric polarization in multiferroic CuFeO_2 ; Appl. Phys. Lett. 97, 094103 (2010).
- [30] Ye, F., Y. Ren, Y., Q. Huang, J. A. Fernandez-Baca, Pengcheng Dai, J. W. Lynn, and T. Kimura, Multiferroic phase of doped delafossite CuFeO_2 identified using inelastic neutron scattering., Phys. Rev. B 73, 220404 (2006)
- [31] Fishman, R. S., Gregory Brown, and Jason T. Haraldsen, Monte Carlo and variational calculations of the magnetic phase diagram of CuFeO_2 ; Phys. Rev. B 85, 020405(R) (2012).
- [32] Terada, N., Yoshinori Tsuchiya, and Hideaki Kitazawa, Magnetic correlations and the influence of atomic disorder in frustrated isosceles triangular lattice antiferromagnet CuMnO_2 . Phys. Rev. B 84, 064432 (2011)
- [33] Ushakov, V.A., Streltsov, V.S., and D. I. Khomskii. Orbital structure and magnetic ordering in stoichiometric and doped crednerite CuMnO_2 . Phys. Rev. B 89, 024406 (2014).
- [34] Ushakov, V.A., Streltsov, V.S., and D. I. Khomskii, Orbital structure and magnetic ordering in stoichiometric and doped crednerite CuMnO_2 ; Phys. Rev. B 89, 024406 (2014)
- [35] Vecchini, C., M. Poienar, F. Damay, O. Adamopoulos, A. Daoud-Aladine, A. Lappas, J. M. PerezMato, L. C. Chapon, and C. Martin. Magnetoelastic coupling in the frustrated antiferromagnetic triangular lattice CuMnO_2 . Phys. Rev. B 82, 094404 (2010).
- [36] Poienar, M., C. Vecchini, G. Andr. A. Daoud-Aladine, Margiolaki, A. Maignan, A. Lappas, L. Chapon, M. Hervieu, F. Damay, and C. Martin; Substitution Effect on the Interplane Coupling in Crednerite: the $\text{Cu}_{1.04}\text{Mn}_{0.96}\text{O}_2$ Case. Chem. Mater. 2011, 23, 85–94 85.

- [37] Ovidiu Garlea, V., Andrei T. Savici, and Rongying Jin., Tuning the magnetic ground state of a triangular lattice system $\text{Cu}(\text{Mn}_{1-x}\text{Cu}_x)\text{O}_2$. *Phys. Rev. B* 83, 172407 (2011)
- [38] Terada, N., Y. Tsuchiya, and H. Kitazawa; Magnetic correlations and the influence of atomic disorder in frustrated isosceles triangular lattice antiferromagnet CuMnO_2 . *Phys. Rev. B* 84, 064432 (2011)
- [39] Damay, F., M. Poienar, C. Martin, A. Maignan, J. Rodriguez-Carvajal, G. Andre and J. P. Doumerc., Spin-lattice coupling induced phase transition in the $S=2$ frustrated antiferromagnet CuMnO_2 . *Phys. Rev. B* 80, 094410 (2009).
- [40] Hiraga, H., T. Fukumura, A. Ohtomo, T. Makino, A. Ohkubo, H. Kimura, and M. Kawasaki., Optical and magnetic properties of CuMnO_2 epitaxial thin films with a Delafossite-derivative structure. *Appl. Phys. Lett.* 95, 032109 (2009).
- [41] Landau, L. D. and Lifshitz, E. M., *Electrodynamics of continuous media*, Fizmatgiz, Moscow, 1959.
- [42] Dzyaloshinskii, I. E., On the magneto-electrical effect in antiferromagnets, *Sov. Phys. JETP* 10, 628-629, 1960.
- [43] Astrov, D. N., The magnetoelectric effect in antiferromagnetics, *Sov. Phys. JETP* 11, 708-709, 1960.
- [44] Folen, V. J., Rado, G. T. and Stalder, E. W., Anisotropy of the magnetoelectric effect in Cr_2O_3 , *Phys. Rev. Lett.* 6, 607-608, 1961.
- [45] Rado, G. T., Magnetoelectric evidence for the attainability of time-reversed antiferromagnetic configurations by metamagnetic transitions in DyPO_4 , *Phys. Rev. Lett.* 23, 644-647, 1969.
- [46] Gorodetsky, G., Sayar, M. and Shtrikman, S., The magnetoelectric effect in the antiferromagnet FeSb_2O_4 , *Mater. Res. Bull.* 5, 253-255, 1970.
- [47] Rado, G. T., Observation and possible mechanisms of magnetoelectric effects in a ferromagnet, *Phys. Rev. Lett.* 13, 335-337, 1964.
- [48] Asher, E., Rieder, H., Schmid, H. and Stossel, H., Some Properties of Ferromagnetoelectric Nickel-Iodine Boracite, $\text{Ni}_3\text{B}_7\text{O}_{13}\text{I}$, *J. Appl. Phys.* 37, 1404-1405, 1966.
- [49] Santoro, R. P., Segal, D. J. and Newnham, R. E., Magnetic properties of LiCoPO_4 and LiNiPO_4 , *J. Phys. Chem. Solids* 27, 1192-1193, 1966.
- [50] Watanabe, T. and Kohn, K., Magnetoelectric effect and low temperature transition of $\text{PbFe}_{0.5}\text{Nb}_{0.5}\text{O}_3$ single crystal, *Phase Trans.* 15, 57-68, 1989.
- [51] Krichevstov, B. B., Pavlov, V. V., Pisarev, R. V. and Selitsky, A. G., *Ferroelectrics* 161, 65-71, 1994.
- [52] Schmid, H., On a magnetoelectric classification of materials, *Int. J. Magn.* 4, 337-361, 1973.

-
- [53] Rivera, J. P., The linear magnetoelectric effect in LiCoPO₄ revisited, *Ferroelectrics* 161, 147-164, 1994.
- [54] Krichevtsov, B. B., Pavlov, V. V. and Pisarev. R. V., Giant linear magnetoelectric effect in garnet ferrite films, *JETP Lett.* 49, 535-538, 1989.
- [55] Rado, G. T., Ferrari, J. M. and Maisch, W. G., Magnetoelectric susceptibility and magnetic symmetry of magnetoelectrically annealed TbPO₄, *Phys. Rev. B* 29, 4041-4048, 1984.
- [59] Schmid, H., Multi-ferroic magnetoelectrics, *Ferroelectrics* 162, 317-338, 1994.
- [57] Smolenskii, G. A. and Chupis, I. E., Ferroelectromagnets, *Sov. Phys. Usp.* 25, 475-493, 1982.
- [58] Khomskii, D., Classifying multiferroics: Mechanisms and effects, *Physics* 2, 20-27, 2009.
- [59] Hill, N. A., Why Are There so Few Magnetic Ferroelectrics?, *J. Phys. Chem. B* 104, 6694-6709, 2000.
- [60] W. Eerenstein, N. D. Mathur and J. F. Scott; Multiferroic and magnetoelectric materials; *Nature* 442, 759-765, 2006.
- [61] Giovannetti, G.; Stroppa, A.; Picozzi, S.; Baldomir, D.; Pardo, V.; Blanco Canosa, S.; Rivadulla, F.; Jodlauk, S.; Niermann, D.; Rohrkamp, J.; Lorenz, T.; Hemberger, J.; Streltsov, S.; Khomskii, D.I., Dielectric properties and magnetostriction of the collinear multiferroic spinel CdV₂O₄, *Phys. Rev. B* 2011, 83, 060402, 2011.
- [62] Zhang, Q.; Singh, K.; Guillou, F.; Simon, Ch.; Bréard, Y.; Caignaert, V.; Hardy, V., Ordering process and ferroelectricity in a spinel derived from FeV₂O₄, *Phys. Rev. B* , 85, 054405, 2012
- [63] Yamasaki, Y.; Miyasaka, S.; Kaneko, Y.; He, J. P.; Arima, T.; Tokura, Y., Magnetic reversal of the ferroelectric polarization in a multiferroic spinel oxide. *Phys. Rev. Lett.* 96, 207204, 2006.
- [64] Singh, K.; Maignan, A.; Simon, Ch.; Martin, C. FeCr₂O₄ and CoCr₂O₄ spinels: Multiferroicity in the collinear magnetic state? *Appl. Phys. Lett.* 2011, 99, 172903.
- [65] Maignan, A.; Martin, C.; Singh, K.; Simon, Ch.; Lebedev, O. I.; Turner, S. J., From spin induced ferroelectricity to dipolar glasses: Spinel chromites and mixed delafossites, *Solid State Chem*, 195, 41(2012).
- [66] Goto, T.; Kimura, K.; Lawes, G.; Ramirez, A. P.; Tokura, Y., Ferroelectricity and Giant Magnetocapacitance in Perovskite Rare-Earth Manganites, *Phys. Rev. Lett.* 92, 257201, 2004.
- [67] Seki, S.; Onose, Y.; Tokura, Y., Spin-Driven Ferroelectricity in Triangular Lattice Antiferromagnets ACrO₂ (A = Cu, Ag, Li, or Na). *Phys. Rev. Lett.* 101, 067204, (2008).

- [68] Hur, N.; Park, S.; Sharma, P. A.; Guha, S.; Cheong, S. W., Colossal Magnetodielectric Effects in DyMn_2O_5 , *Phys. Rev. Lett.*, 93, 107207, (2004).
- [69] Lee, N.; Vecchini, C.; Choi, Y. J.; Chapon, L. C.; Bombardi, A.; Radaelli, P. G.; Cheong, S. W. Giant Tunability of Ferroelectric Polarization in GdMn_2O_5 , *Phys. Rev. Lett.* 2013, 110, 137203.
- [70] Peeks, N. J.; Johnson, R. D.; Martin, C.; Chapon, L. C.; Radaelli, P. G., Magneto-orbital helices as a route to coupling magnetism and ferroelectricity in multiferroic $\text{CaMn}_7\text{O}_{12}$, *Nat. Commun.* 2012, 3, 1277.
- [71] Heyer, O.; Hollman, N.; Klassen, I.; Jodlank, S.; Bohaty, L.; Becker, P.; Mydosh, J. A.; Lorenz, T.; Khomskii, D., A new multiferroic material: MnWO_4 *J. Phys.: Condens. Matter* 2006, 18, L471.
- [72] Rado, G. T., Observation and Possible Mechanisms of Magnetoelectric Effects in a Ferromagnet, *Phys. Rev. Lett.* 1964, 13, 335.
- [73] Furukawa, N.; Sakai, H.; Taguchi, Y.; Arima, T.; Tokura, Y., Composite domain walls in a multiferroic perovskite ferrite. *Nat. Mater.* 2009, 8, 558.
- [74] Kimura, T.; Laskley, J. C.; Ramirez, A. P., Inversion-symmetry breaking in the noncollinear magnetic phase of the triangular-lattice antiferromagnet CuFeO_2 , *Phys. Rev. B*, 2006, 73, 220401(R).
- [75] Terada, N.; Mitsuda, S.; Fujii, T.; Soejima, K.; Doi, I.; Katori, H. A.; Noda, Y., Magnetic Phase Diagram of the Triangular Lattice Antiferromagnet $\text{CuFe}_{1-x}\text{Al}_x\text{O}_2$. *J. Phys. Soc. Jpn.* 2005, 74, 2604.
- [76] Terada, N.; Nakajima, T.; Mitsuda, S.; Kitazawa, H.; Kaneko, K.; Metoki, N., Ga-substitution-induced single ferroelectric phase in multiferroic CuFeO_2 . *Phys. Rev. B* 2008, 78, 014101.
- [77] Pachoud, E.; Martin, C.; Kundys, B.; Simon, Ch.; Maignan, A. J., Effect of Spin Dilution on the Magnetic State of Delafossite CuFeO_2 with an $S = 5/2$ Antiferromagnetic Triangular Sublattice. *J. Solid State Chem.* 2010, 183, 344.
- [78] Kimura, T.; Lawes, G.; Ramirez, A. P., Electric Polarization Rotation in a Hexaferrite with Long-Wavelength Magnetic Structures. *Phys. Rev. Lett.*, 94, 137201(2005).
- [79] Ishiwata, S.; Taguchi, Y.; Murakawa, H.; Onose, Y.; Tokura, Y. Low-magnetic-field control of electric polarization vector in a helimagnet. *Science*, 319, 1643(2008)
- [80] Kitagawa, Y.; Hiraoka, Y.; Honda, T.; Ishikura, T.; Nakamura, H.; Kimura, T. Low-field magnetoelectric effect at room temperature. *Nat. Mater.*, 9, 797(2010)
- [81] Tokunaga, Y.; Kaneko, Y.; Okuyama, D.; Ishiwata, S.; Arima, T.; Wakimoto, S.; Kakurai, K.; Taguchi, Y.; Tokura, Y. Multiferroic M-type hexaferrites with a room-temperature conical state and magnetically controllable spin helicity. *Phys. Rev. Lett.* 2010, 105, 257201.

- [82] Kundys, B.; Maignan, A.; Simon, Ch. Multiferroicity with high- T_c in ceramics of the YBaCuFeO_5 ordered perovskite. *Appl. Phys. Lett.*, 94, 072506 (2009).
- [83] Kawamura, Y.; Kai, T.; Satomi, E.; Yasui, Y.; Kobayashi, Y.; Sato, M.; Kakurai, K., High Temperature Multiferroic State of RBaCuFeO_5 ($R = \text{Y, Lu, and Tm}$). *J. Phys. Soc. Jpn.*, 79, 073705. (2010)
- [84] Choi, Y. J.; Yi, H. T.; Lee, S.; Huang, Q.; Kiryukhin, V.; Cheong, S. W., Ferroelectricity in an Ising Chain Magnet. *Phys. Rev. Lett.* 2008, 100, 047601.
- [85] Yi, H. T.; Choi, Y. J.; Lee, S.; Cheong, S. W. Multiferroicity in the square-lattice antiferromagnet of Ba_2CoGe_2 . *Appl. Phys. Lett.* 2008, 92, 212904.
- [86] Akaki, M.; Tozawa, J.; Akahoshi, D.; Kuwahara, H. Gigantic magnetoelectric effect caused by magnetic-field-induced canted antiferromagnetic-paramagnetic transition in quasi-two-dimensional $\text{Ca}_2\text{CoSi}_2\text{O}_7$ crystal. *Appl. Phys. Lett.* 2009, 94, 212904.
- [87] Rivera, J. P., The linear magnetoelectric effect in LiCoPO_4 . Revisited., *J. Ferroelectrics* 1994, 161, 147.
- [88] Singh, K.; Caignaert, V.; Chapon, L. C.; Pralong, V.; Raveau, B.; Maignan, A., Spin-assisted ferroelectricity in ferrimagnetic $\text{CaBaCo}_4\text{O}_7$. *Phys. Rev. B* 2012, 86, 024410.
- [89] Lawes, G.; Harris, A. B.; Kimura, T.; Rogado, N.; Cava, R. J.; Aharony, A.; Entin-Wohlman, O.; Yildirim, T.; Kenzelmann, M.; Broholm, C.; Ramirez, A. P. Magnetically Driven Ferroelectric Order in $\text{Ni}_3\text{V}_2\text{O}_8$. *Phys. Rev. Lett.* 2005, 95, 087205.
- [90] Kimura, T.; Sekio, Y.; Nakamura, H.; Siegrist, T.; Ramirez, A. P. Cupric oxide as an induced-multiferroic with high- T_C . *Nat. Mater.* 2008, 7, 291–294.
- [91] Naito, Y.; Sato, K.; Yasui, Y.; Kobayashi, Y.; Kobayashi, Y.; Sato, M. Ferroelectric Transition Induced by the Incommensurate Magnetic Ordering in LiCuVO_4 . *J. Phys. Soc. Jpn.* 2007, 76, 023708.
- [92] A. H. Arkenbout, T. T. M. Palstra, T. Siegrist, and T. Kimura Ferroelectricity in the cycloidal spiral magnetic phase of MnWO_4 . *Phys. Rev. B.* 74, 184431 (2006)
- [93] Tokura Y. and Seki S.; Multiferroics with spiral spin orders. *Adv Mater.* 221554-65(2010)
- [94] S. W. Cheong and M. Mostovoy, Multiferroics: a magnetic twist for ferroelectricity, *Nature Materials*, 6, 1, 13–20, (2007).
- [95] H. Katsura, N Nagaosa, Alexander and V. Balatsky; Spin Current and Magnetoelectric Effect in Noncollinear Magnets., *Phys. Rev. Lett.*, 95, 057205(2005).

-
- [96] Stephen Blundell, Magnetism in condensed matter; Oxford master series in condensed matter physics.
- [97] W. H. Meiklejohn and C. P. Bean, Phys. Rev. 105, 904 (1957).
- [98] E. C. Stoner and E. P. Wohlfarth, Nature 160, 650 (1947).
- [99] E. C. Stoner and E. P. Wohlfarth, Philosophical Transactions of the Royal Society of London. Series A, Mathematical and Physical Sciences 240, 599 (1948).
- [100] Nogues, J. and Ivan K Schuller; Exchange bias; Journal of Magnetism and Magnetic Materials; 192, 2, 203–232 (1999).
- [101] Review: W.H. Meiklejohn, J. Appl. Phys. 33, 1328(1962)
- [103] Meiklejohn W.H., C.P. Bean, Phys. Rev. 102, 1413(1956)
- [104] Anand V. K., D. T. Adroja, and A. D. Hillier; Ferromagnetic cluster spin-glass behavior in PrRhSn₃; Phys Rev B 85, 014418 (2012)
- [105] Vogel H., Phys. Z. 22, 645 (1921).
- [106] Souletie J. and J. L. Tholence, Phys. Rev. B 32, 516(R) (1985).
- [107] Krivoruchko V. N.; Griffiths phase and the metal-insulator transition in substituted manganites; Low Temp. Phys. 40, 586 (2014).
- [108] Bray A. J. and M .A. Moore; On the eigenvalue spectrum of the susceptibility matrix for random spin systems; J. Phys. C: Solid State Phys., 15,765-771 (1982)
- [109] J. Deisenhofer, D. Braak, H.A. Krug von Nidda, J. Hemberger, R. M. Eremina, V. A. Ivanshin, A. M. Balbashov, G. Jug, A. Loidl, T. Kimura, and Y. Tokura;Phys. Rev. Lett. 95, 257202 (2005)
- [110] Giauque, W. F., A thermodynamic treatment of certain magnetic effects. a proposed method of producing temperatures considerably below 1° absolute, J. Amer. Chem. Soc., 49, 1864-1870, 1927.
